

Alma Mater Studiorum – Università di Bologna

**DOTTORATO DI RICERCA IN
Ingegneria Elettrotecnica**

Ciclo XXIX

Settore Concorsuale di afferenza: 09/E2

Settore Scientifico disciplinare: ING-IND 33

**PHYSICS OF ELECTRICAL TREEING IN
SILICONE GEL**

Presentata da: Paolo Mancinelli

Coordinatore Dottorato:

prof. **Domenico Casadei**

Relatore:

prof. **Andrea Cavallini**

Esame finale anno 2017

TABLE OF CONTENTS

I	THE THESIS WORK	3
II	SILICONE GEL	5
II-1	POLYSILOXANES.....	5
II-1.1	<i>GENERAL CHARACTERISTICS</i>	5
II-1.2	<i>APPLICATIONS</i>	9
II-1.3	<i>SILICONE GEL PECULIARITIES</i>	10
II-2	POWER MODULES ENCAPSULATION.....	11
II-3	CABLE JOINTS	15
III	PARTIAL DISCHARGE AND ELECTRICAL TREEING	18
III-1	PARTIAL DISCHARGES	18
III-1.1	<i>PARTIAL DISCHARGE PHYSICS</i>	19
III-1.2	<i>PARTIAL DISCHARGES DETECTION AND IDENTIFICATION</i>	21
III-2	ELECTRICAL TREEING IN SOLIDS.....	26
III-2.1	<i>TREE SHAPE</i>	26
III-2.2	<i>TREE GROWTH STAGES AND PD</i>	29
III-2.3	<i>ELECTRICAL TREE ON SILICONE GEL: PREVIOUS RESEARCHES</i>	35
IV	SAMPLE PRODUCTION AND EXPERIMENTAL SETUP	38
IV-1	SAMPLE MANUFACTURING	38
IV-2	EXPERIMENTAL SETUP	42

IV-2.1	MEASUREMENT CELL AND INSTRUMENTS	42
IV-2.2	TEST PROCEDURE.....	44
V	TREE INCEPTION TESTS.....	47
V-1	INCEPTION IN SILICONE GEL	47
V-1.1	<i>SINUSOIDAL AND SQUARE COMPARISON.....</i>	<i>52</i>
V-1.2	<i>HIGH SLEW RATE.....</i>	<i>56</i>
V-1.3	<i>UNIPOLAR SQUARE VOLTAGE.....</i>	<i>57</i>
V-2	INCEPTION IN ELASTOMER	60
VI	TREE INITIATION MODEL.....	63
VI-1	SPACE CHARGE INJECTION	63
VI-2	CHARGE INJECTION MODEL	65
VI-3	CHARGE INJECTION CALCULATION.....	68
VI-4	TREE INCEPTION MODEL	73
VI-5	MODEL VALIDATION.....	77
VII	ELECTRICAL TREE GROWTH.....	82
VII-1	TIME AND LENGTH OF TREES	82
VII-1.1	<i>TIME TO BREAKDOWN (TTB).....</i>	<i>83</i>
VII-1.2	<i>MAXIMUM LENGTH AND FRACTAL NUMBER</i>	<i>86</i>
VII-2	GROWTH MECHANISM IN GEL.....	90
VIII	CONCLUSIONS	96
	REFERENCES	99

I THE THESIS WORK

The silicone gel use as electrical insulator is undoubtedly linked to the power electronic modules encapsulation. The combination of good thermal stability, electrical insulation, and mechanical characteristics is the reason of this link as it will be better explained in the next pages. Today, power modules encapsulation is still the major application of this material, even if other are growing of relevance, such as the insulation in cable joints. However, the progress of the technology in the power modules have been the triggering factor for several studies on the properties of this material.

The increase of the operation voltage in power electronic modules brought a consequent increase of the electrical stress on the silicone gel used. In particular, the small size of the diodes and of the corners of the baseplate or the metallization causes very high field in particular areas. This is the classical condition for partial discharges and for a destructive degradation of the insulation such as the electrical treeing. The electrical trees have been deeply investigated in solid dielectric since the 70's, but the behavior in the gel, that shows characteristics of both solid and liquid materials, is strongly different, as it will be explained in this work.

This thesis divides the study on the electrical treeing into two main phases: the inception and the growth. Both are carried out assessing the influence of the waveform frequency and shape on the electrical treeing. The analysis of the tree inception, which is the initial stage of the tree, have a primary importance since it permits to evaluate the reasons and the conditions generating the tree. In this work, it is proposed a physical model explaining the mechanism of the inception,

supported by a numerical calculation and verified through the experimental tests carried out.

The study of the electrical tree growth furnishes a knowledge of the rapidity and of the type of damage produced by the tree. In the particular case of the silicone gel, the evaluation of the growth permits to understand several peculiar features of this material, which make it highly different from solids.

Although the electrical treeing is a well-known degradation in solids, it is not the same for gels. Therefore, this work wants to achieve the same level of understanding of the electrical treeing mechanism reached in solids also in gels.

II SILICONE GEL

II-1 POLYSILOXANES

The term “silicone” was chosen before the IUPAC rules by analogy with “ketone”. At that time, it was thought that the chemistry of silicone could have important analogies to the chemistry of carbon. The reason is, indeed, the similarity of the structural unit of the silicone base chain R_2SiO with the ketone R_2CO . According to IUPAC rules, the scientifically correct name for silicones is polyorganosiloxanes, from the siloxane chemical group Si-O-Si. Nevertheless, the term “silicones” is today commonly used for compounds in which silicon atoms are linked via oxygen atoms, where each silicon atom bearing one or several organic groups [1].

II-1.1 General characteristics

Polysiloxanes present some peculiar features deriving from their general structure:

1. They are polymeric and they have the typical structural form of organic macromolecules.
2. They contain silicon-oxygen bonds, thus they have the same units of the structure forming silicates and silicic acids.
3. They contain hydrocarbon radicals linked directly to silicon and, therefore, they are correlated to organic chemistry.

For these features, silicones can be considered in an intermediate position between the inorganic and the organic compounds, with similitudes with both silicates and organic polymers. This dual nature causes the particular fascination of this class of compounds.

A great variety of compounds is attainable in polyorganosiloxane chemistry. Indeed, different siloxane units can be combined with one another in the same molecule, leading to compounds with significant macroscopic differences. The various siloxane units can be divided according to the number of oxygen atoms bonded to the silicon one. Therefore, a single siloxane unit can be monofunctional (M), difunctional (D), trifunctional (T), or even tetrafunctional (Q) [2] as shown in Figure II-1.

Starting compound	Structural unit		Application
	Symbol	Functionality	
(CH ₃) ₃ SiCl Monochloro- trimethylsilane	M	$\begin{array}{c} \text{CH}_3 \\ \\ \text{H}_3\text{C}-\text{Si}-\text{O}_{0.5} \\ \\ \text{CH}_3 \end{array}$ monofunctional	chain end in silicone fluids, trimethylsilyl protecting groups
(CH ₃) ₂ SiCl ₂ Dichlorodi- methylsilane	D	$\begin{array}{c} \text{CH}_3 \\ \\ \text{H}_3\text{C}-\text{Si}-\text{O}_{0.5} \\ \\ \text{O}_{0.5} \end{array}$ difunctional	linear siloxane polymers, silicone fluids, rubbers, elastomers
CH ₃ SiCl ₃ Trichloro- methylsilane	T	$\begin{array}{c} \text{O}_{0.5} \\ \\ \text{H}_3\text{C}-\text{Si}-\text{O}_{0.5} \\ \\ \text{O}_{0.5} \end{array}$ trifunctional	silicone resins for paints, impregnating agents, masonry protection
SiCl ₄ Tetrachloro- silane	Q	$\begin{array}{c} \text{O}_{0.5} \\ \\ \text{O}_{0.5}-\text{Si}-\text{O}_{0.5} \\ \\ \text{O}_{0.5} \end{array}$ tetrafunctional	silicone resins

Figure II-1: Origin compound, functionality, and fields of application of silicone structural units from [2]

Different composition of siloxane units may produce significantly different silicone products. Linear silicone fluids are composed mainly of D units, which give closed rings in combination with one another. The base polymers for silicone

elastomers or silicone rubbers consist of D units that bear cross-linkable functional groups. The main structural features of the highly branched silicone resins are T units, often combined with D units to make the resins more flexible. Silicone resins can also contain Q and M units. Actually, it is also possible to use combinations of three or four different types to construct a molecule, thus numerous silicone products can be synthesized and small ratio variations can significantly influence the final result. Despite the difference between the silicones, they have common properties:

- A significant thermal stability and thermal resistance at high temperature, e.g. silicone elastomers have the widest operating temperature range of commercially important rubbers;
- Low chemical reactivity with high oxidation resistance;
- Anti-stick capability and good adhesion to surfaces with hydroxyl groups;
- Low toxicity;
- Low thermal conductivity, but it can be increased by a large amount of inert fillers;
- The ability to repel water and form watertight seals;
- Good resistance to oxygen, ozone, and UV light;
- Gas Permeability;
- Transparency;
- Good electrical properties: Siloxanes and their mixtures with pyrogenic silica have a very good electrical insulating capacity. The electrical properties are temperature dependent and are strongly affected by exposure to water. In other application, the addition of carbon blacks can decrease strongly the resistivity.

The most common silicon-based organic polymers, in particular for rubbers and fluids, are the polydimethylsiloxanes (PDMS). PDMS are optically clear, and, like the greater part of the silicones, inert, non-toxic, and non-flammable. The chemical formula of PDMS is presented in Figure II-2.

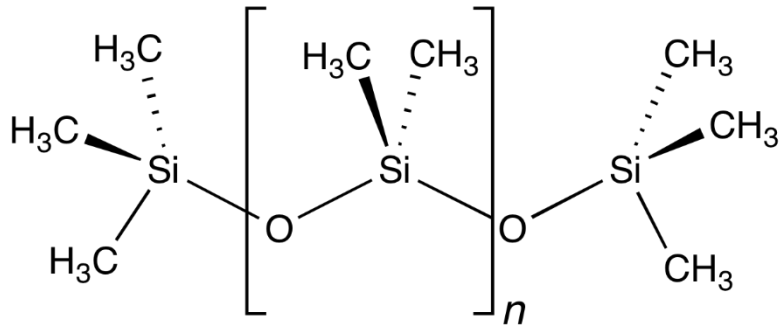


Figure II-2: PDMS structure

Solid silicones can be divided depending on their reticulation temperature or their composition before the cross-linking. Following the first, silicones are divided in room temperature vulcanizing (RTV) or high temperature vulcanizing (HTV). RTV are easier to be employed, especially as sealants, adhesives, or coatings, since they cross-link without the need of a heating source, while HTV are mainly used for industrial scale application in molded objects [2]. From the composition point of view, silicones can be one-component or two-components systems. In the two-components systems, the curing occurs after the mixing of the components, with different ratios, depending on the curing mechanism of the material. In this case, it is important to control the homogeneity of the solution and the correct ratio used, while the process, depending on the environmental condition, should take from few minutes to several hours to be completed. On the other hand, the one-component curing mechanism takes place forming an elastic skin on the surface of the material employed under the action of atmospheric moisture. Curing proceeds from the surface to the inside and the rate of curing depends not only on the ambient temperature and humidity but also on the type of material and the object shape.

II-1.2 Applications

The broad set of properties of silicones leads to a wide range of applications for these materials.

Because of silicone liquids high thermal stability and good low-temperature performance, they are used as heat transfer media in heating circuits in chemical, petrochemical, pharmaceutical, and food industries and in solar power plants, and as refrigerants in cryostats, freeze dryers, and climate simulation plants. The low surface tension of silicone leads to their use as release agents in the processing of plastics and rubber articles and as a lubricant, especially in paste or grease form. Because of their surface activity, polydimethylsiloxanes are employed as antifoams in aqueous systems, in laundry detergents, and in petroleum processing. Silicone oils are important dielectric coolants for transformers and rectifiers because of their flame resistance, resistance to aging, material compatibility, and physiological inertness.

The range of applications of silicone elastomers is even broader than the one of liquids. In electrical insulating devices, silicones are used for cable sheaths, wire insulation, power cable joints, and power cable endcaps. In electronics, silicones are present in various types of coatings and encapsulations. Silicone gel, which is the material studied in this thesis work, have in common several features with elastomers. The main application of this material in the electronic and electric field, such as power module encapsulation and cable joints, will be deeper discussed in the next paragraphs.

Many household products are made by polysiloxanes, such as pot seals, coffeemaker tubes and seals, baby bottle nipples, oven gaskets, and anti-stick papers. Automotive and airplane industry are probably the fields where silicone elastomers are employed within the higher number of components: air bags, window seals, ignition cables, oil pan gaskets, headlight seals, cooling and turbo hoses, vibrational damping, and O-ring are only some of the objects made by silicones and widely employed in these fields. In general, the elastomers are the

form of silicones more often employed in different solutions. Other applications, in fact, range from casting forms, membranes, impression molding compounds, anti-stick bladders, protective masks, etc. Noteworthy are the devices employed in medicine and dentistry, where tooth impression compounds, implants, pumps, heart valve seals, catheters, and lenses are made by silicone elastomers.

Whereas silicone fluids and elastomers are based on linear polymers, silicone resins are highly branched, containing significant quantities of T or Q units, thus, they show a more reticulated solid structure than the other silicones. The main use of these resins is as painting or coating where high thermal stability and good water repellency.

II-1.3 Silicone gel peculiarities

Most potting, filling, or encapsulating materials employed in electrical or electronic applications are either fluid or resinous in nature. A silicone gel is a departure from these types of products. It merges the non-flowable permanence of a solid polymer, with the protection from mechanical and thermal stresses provided by a fluid. Silicone gel temperature range of application is between -65°C and 200°C [3]. The silicone gel tackiness provides mechanical adhesion to almost all the surfaces, and its jelly-like nature provides it the self-healing capability, making it able to recover after mechanical perforation or cut.

Typical silicone gel is a form of silicone rubber and mainly made by PDMS. The gel is usually a RTV material and often consists of two components to be mixed with a ratio close to 1:1. The most common curing reaction, indeed, is due to catalysts consisting of platinum compounds which come together with one of the components [4].

In silicone gels, the combination of the electrical properties, with the peculiar thermo-mechanical behavior makes this dielectric perfect for embedding IGBT modules or for cable joint insulation, where the gel high elasticity, thermal

stability and ability to compensate the mechanical stress caused by temperature changes during device operation are of high importance [5].

II-2 POWER MODULES ENCAPSULATION

Power electronic modules are the equipment providing the physical containment for several power components, mostly power semiconductor devices. Different technologies are today used for power modules and their shape, while the materials employed depend on the power semiconductor number, voltage, and operating conditions [6].

The take-up of electronics in transport systems, which use semiconductor technology to convert and control electrical power, has resulted in tremendous growth in the use of power electronics devices. The number of systems employing these devices is continuously increasing especially in electrical traction applications such as locomotive, subway, elevator, and car [7]. The development of these technologies requires an increase of power density, thus an increase in the maximum operating voltage and current. For example, high voltage IGBT (Insulated Gate Bipolar Transistor) power modules have been produced up to 6.5 kV leading to enhance the performance of dielectric materials used in these modules [8].

Silicone gel is usually employed inside power modules in order to encapsulate power electronic circuits and placed between the circuits and the case, which is made by epoxy resin or plastic material. Indeed, because of the different coefficients of thermal expansion of the involved materials, it is necessary to use a dielectric which can compensate the mechanical stress in power cycling [9]. Moreover, the role of the gel is also to protect components and connections against pollution, moisture, and also to avoid partial discharges (PD, see chapter III for the introduction to partial discharges).

The circuit, in fact, has a complex interior structure. The components inside the module can be at different potential and the voltage in them can vary quickly with waveforms similar to fast square voltage, usually unipolar. Therefore, an inhomogeneous field distribution is present inside the power module case. Consequently, electrical stress degradation is one of the possible failure causes [10]–[12] in power modules and probably the most dangerous in the lately developed high voltage ones [13], [14].

The components which commonly form the power modules can be schematized as in Figure II-3. The ceramic substrate is soldered to a baseplate which ensures the mechanical stability of the assembly and the thermal transfer towards the cold source. From the electrical point of view, the baseplate is electrically connected to the ground, thus the lower face of the substrate is at zero potential. The substrate is required to furnish a common plane for the dies, it should be a dielectric but with good thermal conductivity. Therefore, it is made of an electrically insulating material, such as alumina or aluminum nitride. The chips are connected to the upper face of the substrate, through the metallization which is typically realized by a thick copper layer, either connected to the substrate by a eutectic bonding process or by an active metal brazing process. Finally, the dies are connected externally through copper wires and the whole power electronic circuit is covered by silicone gel.

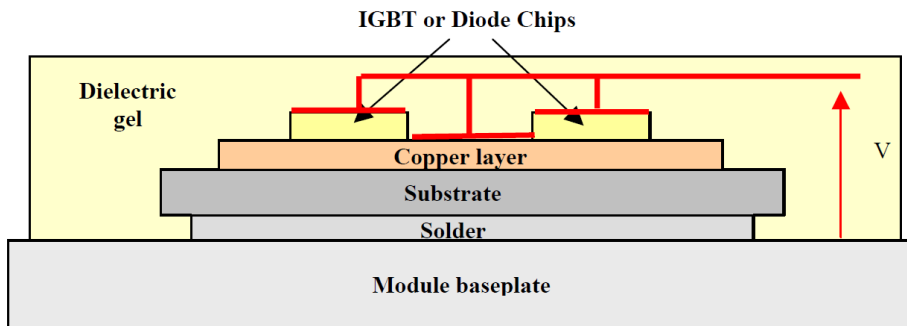


Figure II-3: Generic power module chip arrangement

A series of studies have investigated the electric field inside the power modules, its inhomogeneity, and the possible development of discharges. The finite element method (FEM) has been used to evaluate the electric field in the system [15], [16]. The calculations highlighted the presence of strongly enhanced field at the edge of the metallization, in correspondence of the triple point, between the substrate, the copper, and the silicone gel. Depending on the shape of the copper edge and the relative permittivity of the substrate employed, the electric field can be one or more order of magnitude higher than the one present in the central part of the substrate, where the field is constant.

This relevant inhomogeneity of the electric field inside the silicone gel at the edge of the copper solder can lead to PD, which began the main cause of deterioration of the dielectric gel. When the self-healing properties of the silicone gel are not sufficient to recover this electrical stress, the dielectric can be irreversibly damaged by an electrical tree and a fatal breakdown will follow. The presence of PD have been confirmed experimentally [14], [17], [18] and their location is at the edge of the metallization, as expected after FEM analyses. Figure II-4 and Figure II-5 show the presence of partial discharged detected under different test conditions [15], [18].

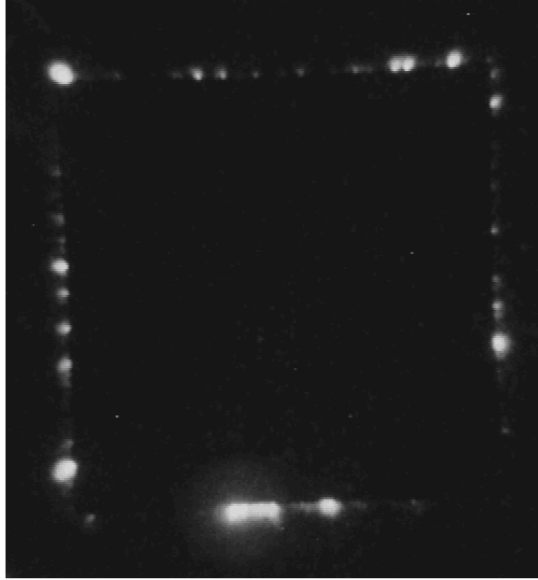


Figure II-4: Light emission during PD activity at the edge of the metallized substrate, thanks to [18]

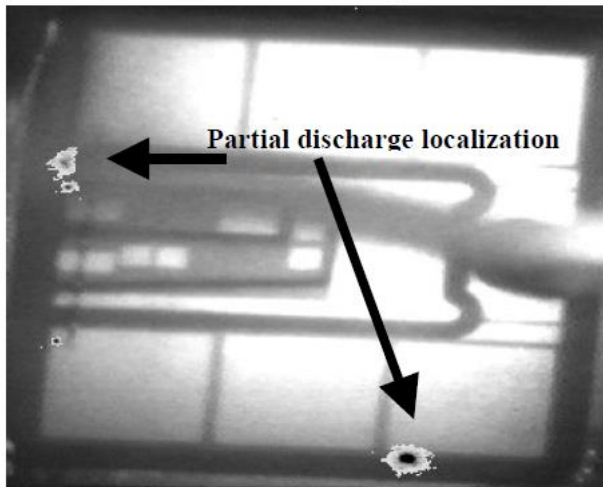


Figure II-5: PD location in a 5 kV test, thanks to [15]

The probability of PD inception in the silicone gel used to encapsulate the power electronic devices grows with the voltage applied. Therefore, in the last years, some researches have been carried out in order to substitute the silicone gel or to enhance its properties [15], [19]–[22]. Despite these researches, a clear

treatise on the physics of phenomenon occurring during the electrical treeing and its correlation with the electrical parameters has not been articulated so far.

II-3 CABLE JOINTS

Another important application of silicone gel as dielectric material is the filling of power cable accessories. They are the most breakable points of power cables since the continuity and homogeneity of the extruded cable are interrupted and the electrical field is distorted. The cable accessories require an expert operator to be correctly mounted and, especially for high voltage applications, stress grading systems, in order to decrease possible electric field enhancements.

The development of silicone gel technology brought the possibility of in-line jointing with high reliability, simple installation procedure, and low installation costs [23], [24]. The alternative medium and low voltage taped joints, indeed, require three layers of rubber tape half-lapped and two layers of plastic tape, with longer installation time and more chances of human error. Common silicone gel splices are usually made by a rigid hinged clamshell housing filled with silicone gel or by a flexible elastomeric wraparound sleeve coated with silicone gel as shown in Figure II-6 [25].



Figure II-6: Silicone gel splices: at the top a clamshell housing at the bottom a wraparound sleeve, before and after installation [25]

The state-of-the-art in low voltage jointing systems has been advanced by the integration of a mechanical connector into a gel closure as shown in Figure II-7. This permits to the gel closure design to be optimized in size and function for set screw mechanical connectors with advantages in ease of installation and puncture resistance over existing closures.

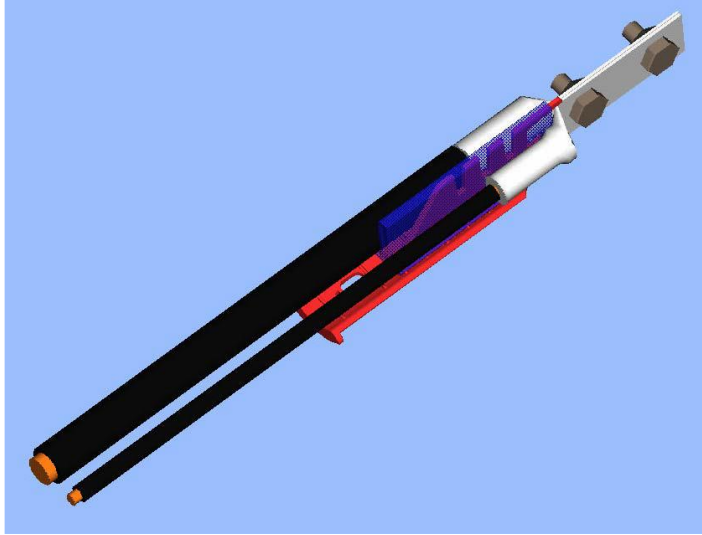


Figure II-7: termination with rigid connector inside [25]

The design voltage of 5 kV has been already reached. The reliability and the simple installation process of the silicone gel joints are leading the manufacturer to use this dielectric in order to fabricate products for higher operating voltage, where the material will be seriously electrically stressed. Therefore, an accurate study on the consequence of PD and electrical treeing in silicone gel will be of interest for the power cable manufacturer too.

III PARTIAL DISCHARGE AND ELECTRICAL TREEING

The PD detection is not present in the main investigations of this thesis work, as it will be clear in the next chapters. This choice has been made after the results of preliminary measurements on solid materials and thanks to the strengthened knowledge of the connection between electrical treeing and PD. Nevertheless, it is not possible to discuss electrical treeing without a sufficient knowledge of PD, which generate the treeing itself. Therefore, a brief explanation of the physic and the detection of PD is made in this chapter, before introducing the electrical treeing phenomenon.

III-1 PARTIAL DISCHARGES

“Partial discharges (PD) are localized electrical discharges that only partially bridge the insulation between conductors and which can or cannot occur adjacent to a conductor. Partial discharges are in general a consequence of local electrical stress concentrations in the insulation or on the surface of the insulation. Generally, such discharges appear as pulses having durations of much less than 1 μs ” [26].

Since the beginning of the 20th century, when high voltages were increasingly used for the long-distance transmission of electrical power, it became

clear that discharges in gas-filled inclusions and defects of solid dielectrics can be the origin of the insulation degradation and of the consequent breakdown. Therefore, the interest around the PD detection grew significantly, developing various tools and employing optical, acoustical, chemical and electrical methods. Since the 1960s, the electrical PD measurement is a widely accepted tool for the quality assurance tests of HV apparatus during operation life [27].

III-1.1 Partial discharge physics

The flow of electric charges is the generation mechanism of discharges. An electron situated near the cathode surface and generated by externally supplied radiation can move toward the anode under the action of the applied field producing more electrons by collisional ionization with gas molecules and, thus, leading to an electron avalanche. Following the propagation mechanism, the avalanches creating PD might be divided into two main processes: the Townsend-like and the streamer-like discharges [28].

The avalanche in Townsend-like discharges is easily described by an exponential law:

$$N(x) = N(0)e^{\alpha x} \quad (1)$$

where N is the number of negative ions in the avalanche, x is the distance from the avalanche starting point and α is the Townsend ionization coefficient, expressing the number of ion pairs generated per unit length by an electron moving from cathode to anode. A schematic representation of the avalanche is presented in Figure III-1.

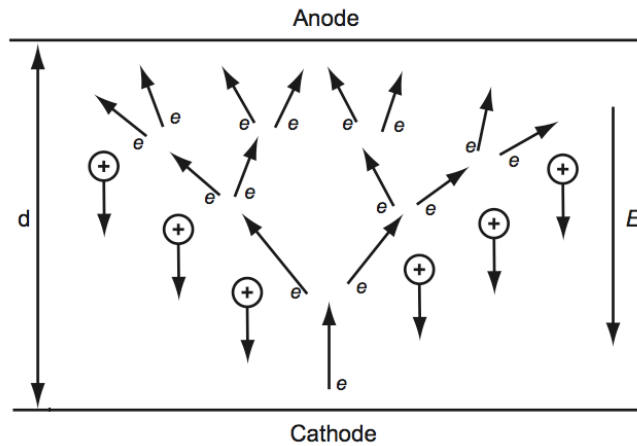


Figure III-1: Townsend discharge avalanche

Due to the avalanche shape, a great part of the electrons is produced close to the anode, which they reach quickly, decreasing the actual electric field inside the gap and consequently the α parameter thus ceasing the electron avalanche itself. Since the electron mobility is much higher than that of the positive ions, the current flowing during the initial buildup of avalanches is largely due to the electron flow, leaving behind the slower positive ions. The positive ions reach the cathode in a longer time window, generating a homogeneous current flow. The overall result is a flat current with an initial peak, which can be significantly pronounced or not, and a duration in the range of the hundreds of nanoseconds. The magnitude of charge usually carried out by a Townsend discharge is low, the rise and fall time of the current are quite long, thus this type of discharges is usually more difficult to be detected, especially in online measurement [29].

Streamer discharges are faster and more energetic than Townsend ones and they are the most common discharges detected in dielectrics. The initial source of discharges is the same i.e. an avalanche of electrons, but, in this case, the space charge due to the avalanche itself is large enough to reach the same order of magnitude of the applied electric field. Consequently, secondary avalanches are generated inside the gap which is quickly short-circuited by a plasma channel. The

current produced by the streamer discharges has very short rise times, in the order of the nanoseconds, and fall time of few tens of nanoseconds. The magnitude of the current is higher than in Townsend-like discharges and can exceed a hundred of milliamps. The classical currents produced by Townsend and streamer discharges are presented in Figure III-2.

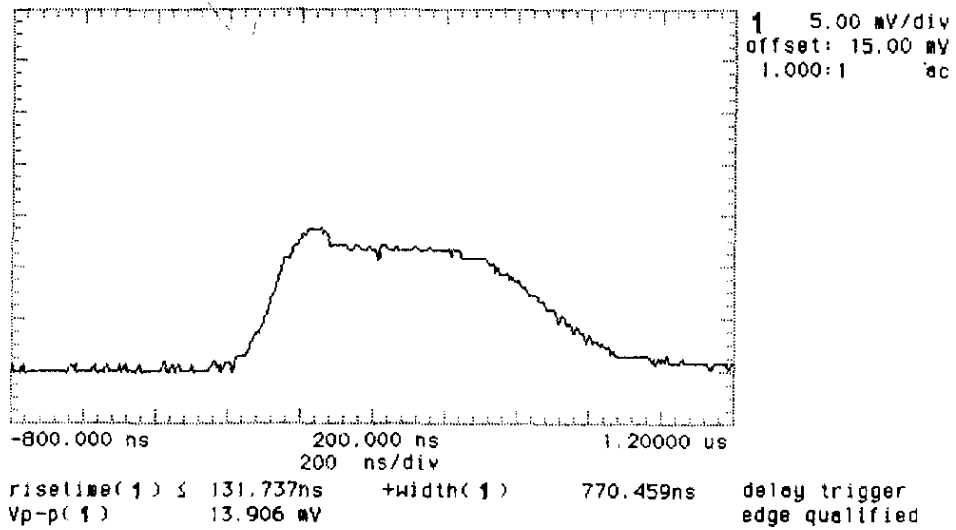
The main parameters influencing the transition between Townsend-like and streamer-like discharges are related to the electric field and the cavity size. The PD physics and this transition mechanism have been widely discussed in the literature and, for a complete discussion, the reader should refer to [30].

III-1.2 Partial discharges detection and identification

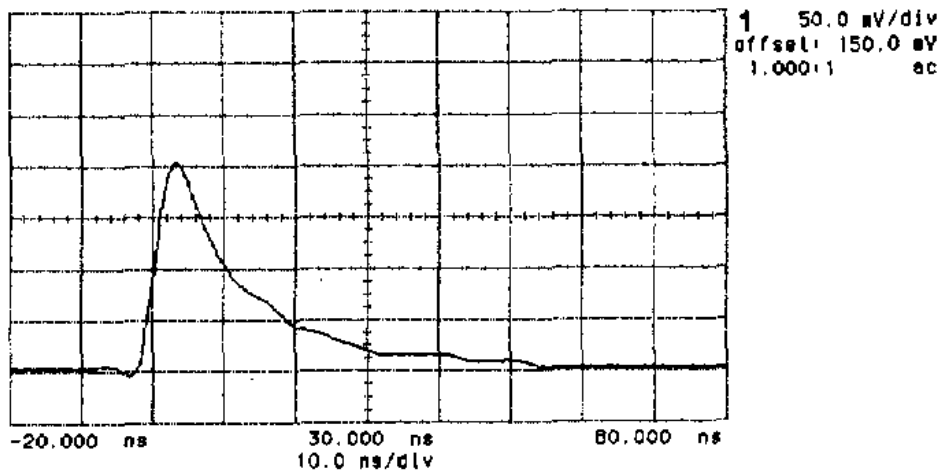
PD measurement methods can take advantage of different PD properties in order to employ various system [26], [27]:

- Electrical conducted signals;
- Electromagnetic radiated fields (using antennas, electric or capacitive couplers);
- Audible sound;
- Ultrasound pressure waves in air or fluids;
- Ultrasound acoustic emission from waves propagating in solid structures (e.g. transformer tanks);
- Light;
- Ultraviolet radiation;
- Chemical byproducts (in air commonly O₃).

Conventional systems detect electrical conducted signals. The measurements reported in the preliminary part of this work were carried out through a PD-base supplied by Techimp, which analyzes electrical conducted signals.



hp stopped



1 5 25.00 mV

Figure III-2: comparison between Townsend (upper) and streamer (lower) discharges [30]

PD are complex events. Every PD event can be considered as a pulse having a large frequency content (from the MHz to the GHz range). The information conveyed by PD in a single PD event is often synthesized in just three numbers: the time length, the phase, and the magnitude.

Since PD are repetitive and stochastic phenomena, their analysis requires an accurate model able to reveal the underlying physical processes. The data are elaborated and collected in PD patterns, which provide the density of PD events in the frequency-charge (f-q) plane. Additionally, signal processing tools are used to separate PD from different sources.

The equipment under test is commonly schematized in the so-called *abc* circuit, shown in Figure III-3. The model represents the insulating material, where the capacitance *c* is the cavity or defect where the PD will occur, *b* is the part of the material in series with *c* and *a* is the remaining part of the dielectric, which can be considered in parallel with the other two capacitances.

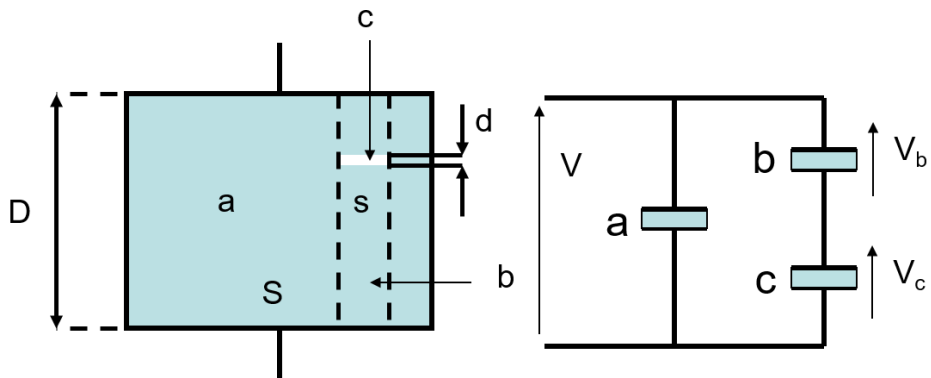


Figure III-3: *abc* circuit for PD representation

The *c* capacitance is much higher than *b*. When *c* is short-circuited by the PD, the charge in the *b* capacitance increases of $V_c b$, where V_c is the voltage applied at the capacitance *c*. This charge is provided by the capacitance *a* and is defined as apparent charge since is not the real charge involved in the PD but a consequence of them. In this process, the current flow happens inside the dielectric and no signal is detected outside. In order to make possible the PD measurement at the terminals of the equipment under test (EUT), a coupling capacitance is commonly employed. Indeed, placing a capacitance much larger than the EUT one, the apparent charge is provided by this coupling capacitance and the current is forced to flow out to the EUT.

The PD detectors, using the electrical conducted signals, can be either a resistor in series with the current path, a coupling capacitance or a high-frequency current transformer (HFCT) measuring the current flowing to ground. Depending on the detector position, the measurement circuit can be direct or indirect, changing the sensitivity of the system and the sign of the charge measured. Moreover, a proper filter for the pulse current generated by the PD should be employed, knowing the EUT characteristics. All these specifications can be found in the already cited standard [26].

Each single PD event is recorded and elaborated by the device used for the detection. The PD are, in fact, rearranged in patterns, highlighting the single pulse properties. These patterns have either two or three axes and show different combination of fundamental characteristics of the PD. Since the PD measurements showed in this work were carried out through a PD-base, the magnitude-phase (which shows also the frequency of repetition through different color in the pattern) and the T-F map (equivalent timelength and frequency) are reported [31], [32]. The possibility to rearrange the pulses into patterns is the only way to analyze a stochastic phenomenon as the PD development. Indeed, PD can occur in various locations inside an insulating system and cause different types of electrical degradation. Analysis of positions and shapes of the PD pulse clusters into the patterns is the only way to identify the defect type and its harmfulness.

The PD identification is mainly carried out following empirical and comparative methods. The pattern analysis should be performed by an expert who is able to interpret the results and classify them. PD sources can be internal, as electrical treeing or due to defects in the insulating material, e.g. voids, delamination, and protrusion or external, as corona or surface discharges. The PD activity due to these processes produces patterns with peculiarities which make them discernable as shown in Figure III-4.

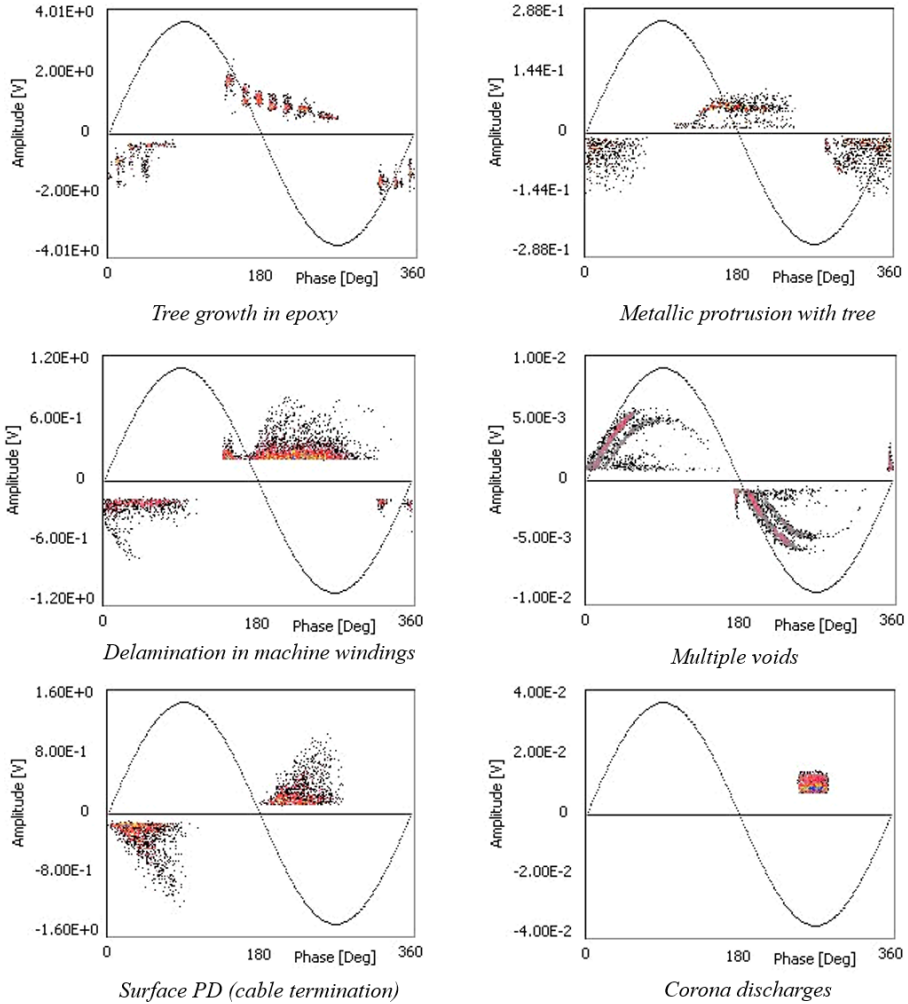


Figure III-4: examples of PD patterns for different degradations

The analysis of PD pulse shape permits to evaluate the distance of the damage from the measurement acquisition system or the dimension of the area interested by the degradation process, which are important features in tests on complex system or online machines. In laboratory tests, as in this work, these became less important, since the test area is well-known, while the accuracy and the sensitivity of the measurements became fundamental. In the next paragraphs, the electrical treeing and its close bond with PD will be better explained.

III-2 ELECTRICAL TREEING IN SOLIDS

The electrical treeing has been known as an electrical breakdown cause for HV insulating systems since the beginning of the last century [33], [34]. It is known to occur in solid materials and it has been observed in both inorganic and polymeric materials. Thus, it must be a process whose mechanism is independent of the chemical nature of the insulation. It has been reported in DC voltage, but it is much more common in AC applications.

It is important to note that water trees [35], [36] will not be treated here. They, indeed, are a different type of dielectric degradation, with substantial difference compared to electrical trees [37].

III-2.1 Tree shape

Electrical trees grow in regions of high electrical stress, such as structural irregularities, metallic asperities or conducting contaminants. Electrical trees which initiate at an electrode growing towards the other are called vented trees, whilst electrical trees generated in the body of the insulation having a branched channel structure roughly oriented along the field lines are defined bow-tie trees. These last are usually originated from impurities or metallic contaminants and should be easier to avoid. On the other hand, vented trees are composed of interconnected hollow tubules with the major channel at the base forming a vent for the whole system which may allow access to the external environment.

Vented trees, which are often more common and dangerous than bow-tie trees, can have different shapes. The terminology used in literature is slightly different depending on the researchers, but the most accepted one divides vented trees into three categories: branched, bush-like, and bush-branch [37]. As shown in Figure III-5, branched trees exhibit a various number of branched structure, made by a series of channels with diameters ranging from few tens of microns to 1 μm in the fine filamentary channels at the tip. In bush-like trees, the channels

are so densely packed that the structure appears like a solid bush-shaped mass when projected in 2D. Finally, bush-branch trees are bush-like trees with branches projecting outside the main bush-like structure.

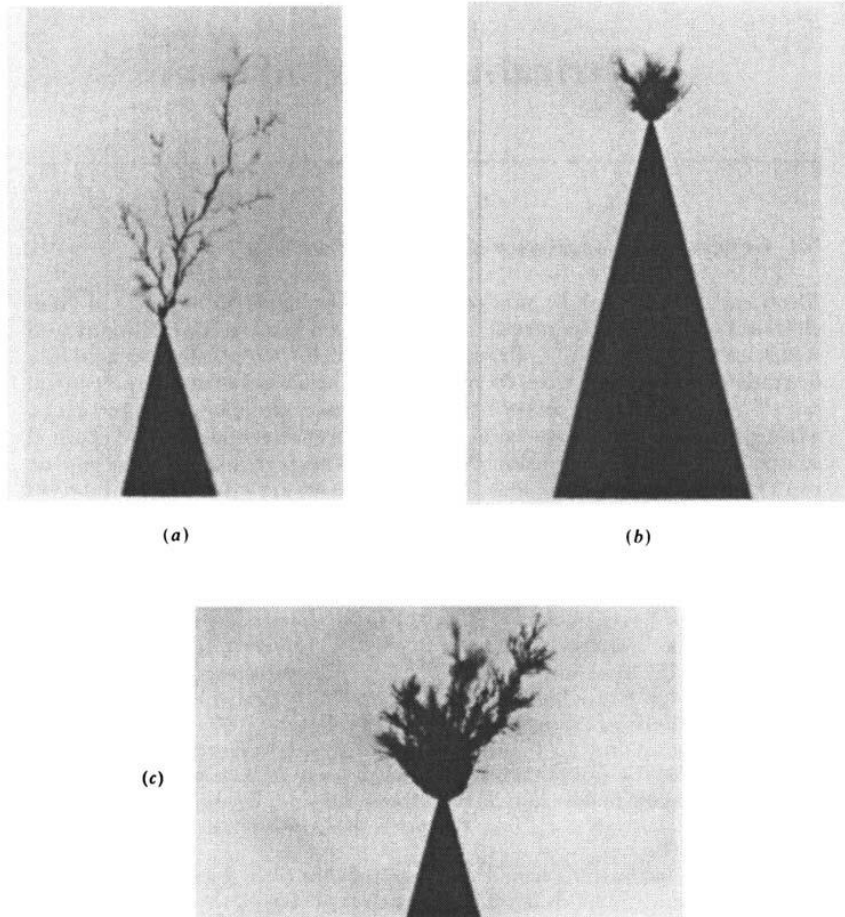


Figure III-5: vented tree shapes: a) branched; b) bush-type; c) bush-branch. Images taken from [37]

The three categories are not completely distinct. In order to better understand the shape of vented trees, the notions of fractal number and fractal structures should be introduced. Indeed, the damage generated by the tree and the tree shape can be characterized by the dimension d_t known as fractal number. To a first approximation, a definition of this quantity can be given by considering the

volume or mass of tree damage $S(L)$, contained within a cube of side L , which is given by [38]:

$$S(L) \propto L^{d_t} \quad (2)$$

Actually, the dimension of any object can be characterized by equation III-1. A cube would have a d_t equal to 3, thus the same of the Euclidean space in which it exists. On the contrary, Fractals are a class of objects whose dimension is less than that of the Euclidean space in which they are present and is usually non-integer.

Electrical tree shape can be considered a statistical fractal [39]–[41]. Contrarily to geometrical fractals which are abstract structures exhibiting exact scale invariance, statistical fractals do not present an exact geometrical scalability, but they exhibit a property, such as their mass $S(L)$, showing a scale invariance, and obeying Equation III-1 with a non-integer value of d_t . In this case, the value d_t assumes the name of fractal number and it can be used to define the tree shape. Bush trees, in fact, have the higher fractal number with d_t higher than 2, branched trees have the smaller fractal number usually up to 1.8 while the bush-branch trees show d_t values in between [42], [43].

The electrical tree shape and its fractal number are determined by different parameters. First of all, electrical trees have been found in many different materials and the material and its characteristics (amorphous phase, glass transition temperature, electrical and mechanical properties, etc.) are parameters which may influence the tree shape. Moreover, the electric field, the frequency, the temperature, and the electrode shape are the more significant variables capable of modifying the fractal number and many empirical correlations are presented in literature in order to connect the electrical stress with the tree shape [37], [38], [43]–[47].

In general, branch trees grow at lower electric field than bush trees and usually the time to create a new branch is almost independent of the field.

Therefore, since the bush trees will have many more branches than a branch tree of the same length, if the time to grow a branch of a specified length is the same, bush trees will grow in length much slower than branch trees. Nevertheless, the damage per unit of volume created by bush trees is sensibly higher than branch trees. In any case, branched trees are usually more dangerous than bush trees as they develop quickly towards the opposite electrode. In many cases, increasing the voltage frequency, the trees tend more to a bush-like shape and usually the grow rate is proportional to frequency.

III-2.2 Tree growth stages and PD

Electrical tree growth is not constant in time. Indeed, it is commonly divided into three main stages [37]:

1. an initial inception stage;
2. a rapid decelerating growth;
3. a final accelerating growth.

In the first stage, commonly named inception or initiation, no physical damage is detectable: in this phase, the electrical field is creating the conditions required to start the tree. The second stage begins with the rapid growth of the first branch, followed by the ramification of the tree, whose growth rate decreases in time. In the last stage, the electrical tree, which has already cross a significant part of the insulation, increases its growth rate reaching quickly the ground electrode.

Figure III-6 shows in a 3D graph the trend of the tree growth in epoxy resin samples applying different voltage. All the curves present a first rapid part, followed by a period with lower growth ratio. This is the decelerating growth stage, followed by a higher slope which represents the final stage. In Figure III-6, the tree growth and its maximum length after 240 min of voltage application decrease increasing the voltage because the tree shape change from branched to

bushy. Finally, for the higher voltage, the specimens suffered breakdown without a proper electrical treeing formation.

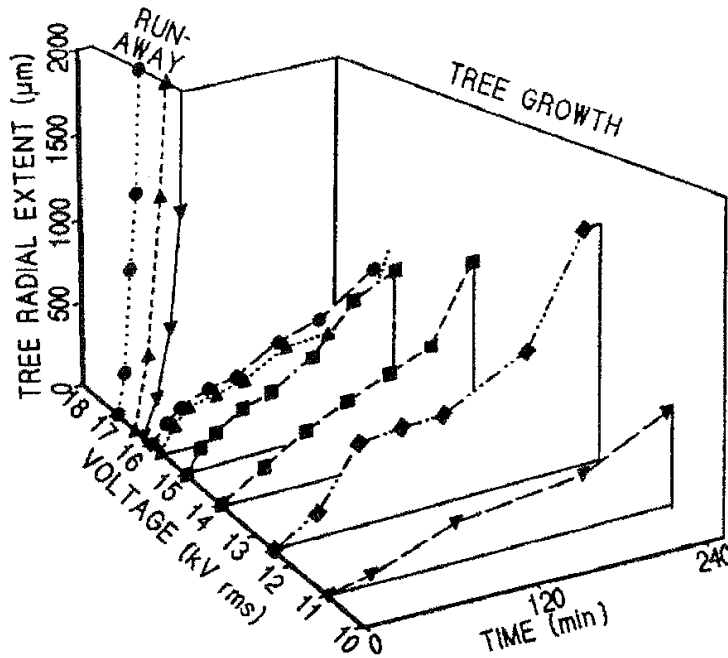


Figure III-6: Tree growth at different voltage applied taken from [38]

Electrical treeing in solid material does not end when the first branch reaches the ground. In order to have a total breakdown, in fact, the hollow channels should increase their diameter. After that the tree crossed the insulation, the electrical degradation, caused by PD, continues to develop, creating few new branches and enlarging the ones already present, until the complete breakdown discharge can find a sufficiently sized path.

While the electrical tree propagation in solids is broadly understood and related to PD action in gas-filled channels or charge injection from conducting channel walls, the inception stage is much less clear. Electrical tree inception is commonly associated with the injection of charge into the polymer [42]. The earliest theories connected the tree initiation to either dielectric heating which would generate a void at the electrode, usually made by a needle in the

experiments, or Maxwell stressing which would cause cracking around the electrode [48]–[51]. Actually, especially in AC voltage, the role of charge injection in the inception stage has been confirmed by the observation of light emission in this initial phase [52]–[54]. These observations have proven to follow well-known charge injection models, such as the Fowler-Nordheim tunneling injection or the Richardson-Schottky injection model, with a direct proportionality between the injected charge and the light emission [55], [56]. Despite the experimental validation, how charge injection supplies the energy to the polymer that causes physical damage essential to the formation of a discharging tubule or channel is not unequivocally ascertained. The impact excitation of molecular species by electrons that have sufficient kinetic energy may initiate a route to chemical degradation or the chemical bonds may be broken by ultraviolet radiation emitted during charge recombination [57], [58].

From an empirical point of view, the tree inception stage has been related to an accumulation of energy or repeated damage. A noteworthy theory by Tanaka and Greenwood [59] states that the time to tree inception is given by the time required for a given amount of energy C_t to be transferred to the polymer:

$$f_{ti}(G_n - G_{th}) = C_t \quad (3)$$

Here G_n is the energy available from the displacement of the injected charge in the local field, and G_{th} is its threshold value for damage producing avalanches, with f_{ti} the number of cycles. The C_t value is dependent on the material properties. Correlating this model to the charge injection and extraction that has been confirmed to occur during the polarity reversal for AC tests, the time to tree inception in solid materials should be inversely proportional to the frequency of the voltage applied.

The decelerating growth stage represents the first stage where the tree is clearly detectable. The gas tunnels development is due to a sequence of PD. This tunnels, which form the electrical tree, can have or not conductive walls, mainly

depending on the dielectric material on which they are growing. The PD in this phase usually present very low energy and they are quite difficult to be detected outside a laboratory setup. Many pieces of work studied the electrical treeing growth analyzing the PD [60]–[65]. The actual length of this second stage is quite difficult to be predicted and it is sensibly influenced by the electrical field and the specimen geometry.

Part of the preliminary analysis of this thesis was carried out on epoxy resin. The aim was to validate a first measurement setup through well-known results. The next figures present in this chapter have been obtained in this first investigation. An example of electrical treeing during the decelerating growth stage is proposed in Figure III-7. The PD-check measurement and the optical images are referring contemporaneously to the same sample, during the tree development. The high sensitivity of the system permitted to detect the very low voltage signal due to PD. In this case, the tree has a branched shape with a very low fractal number in its initial stages, where is barely optically visible.

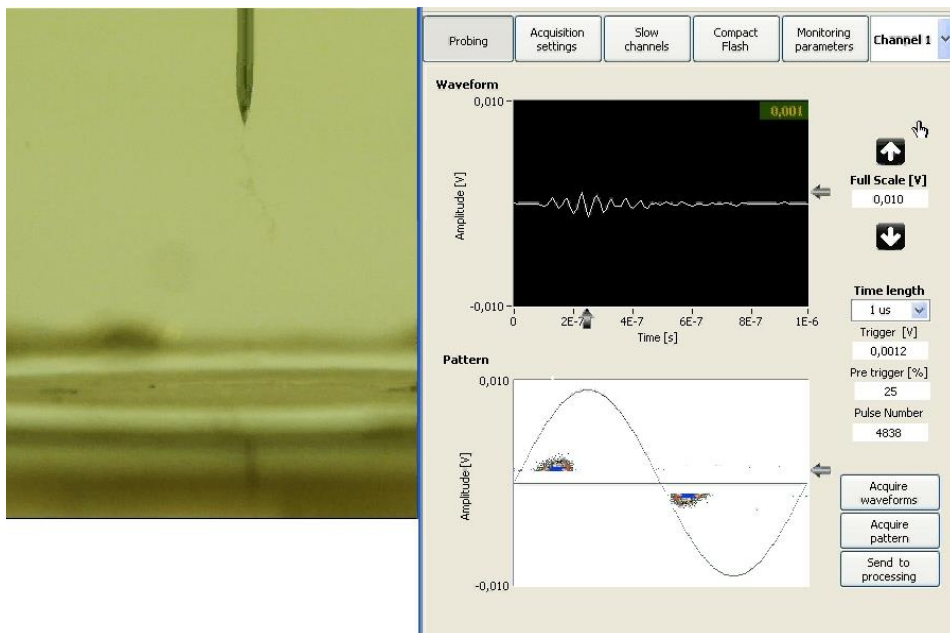


Figure III-7: Decelerating growth stage in epoxy resin

The third stage of the electrical tree, the final accelerating growth is characterized by PD of growing intensity. In this phase, the tree crosses completely the insulation. In bush shaped tree one or two main branches came out from the main structure and, following the electric field, reach the ground. The same branched tree proposed in Figure III-7 showed sensibly higher values of PD in the last part of its growth as presented in Figure III-8. In this last figure, the tree has just reached the ground electrode: from this moment on the PD will continue to enlarge the channels leading to the breakdown.

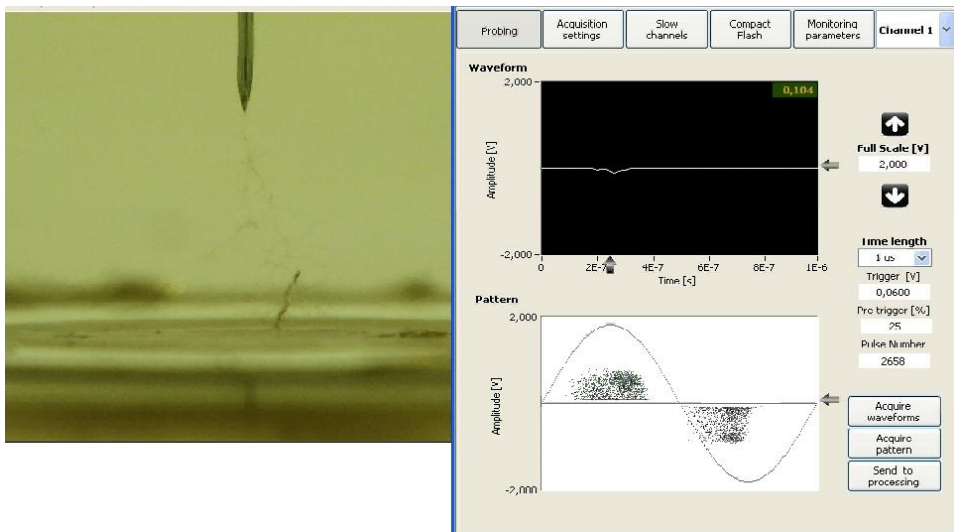


Figure III-8: Final accelerating growth stage in epoxy resin

PD growing the electrical tree, especially in the last stage and in the final pre-breakdown phase, are often cause of significant light emission as shown in Figure III-9.

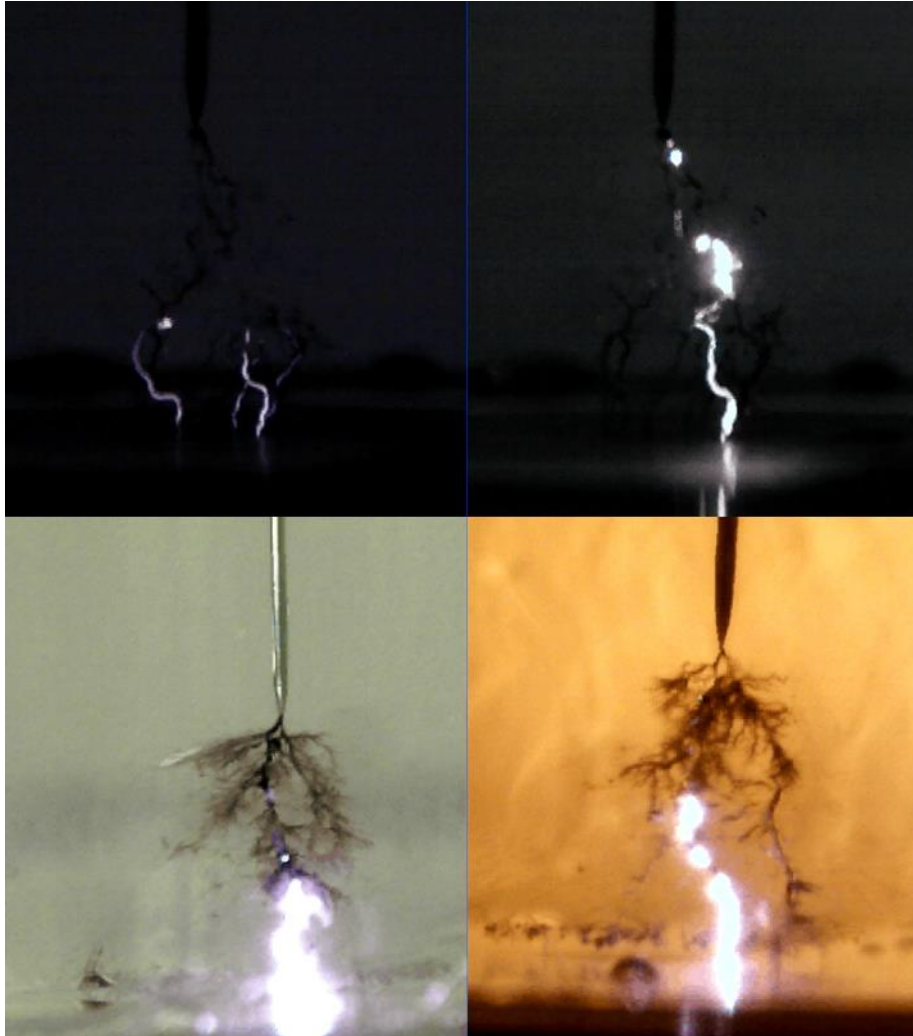


Figure III-9: examples of light emissions during PD in electrical treeing

In the last decade, the studies on electrical treeing focused mainly on improvement of already existing materials, in order to make them able to avoid tree inception or to stop the tree growth. Nanodielectrics are the most promising material for this purpose and several types of research have been carried out in this direction [66]–[68]. Nevertheless, nanodielectrics are often far to obtain the exceptional results desired in industrial scale [69], where they present issues of reliability, safety, and dispersion.

III-2.3 Electrical tree on silicone gel: previous researches

The main applications of silicone gel in HV are relatively recent (see chapter II). For this reason, just few experiments of electrical tree inside this material can be found in the literature. Moreover, the peculiar nature of silicone gel, with reminiscences of both liquid and solid dielectrics, have created two different approaches.

A first series of studies considered the silicone gel as a liquid dielectric [8], [18], [70], [71]. In these pieces of work, the tests were conducted under short pulse voltage, the same way used often to evaluate the performances of dielectric oils, without any electrical tree growth study. Considering the gel as a liquid material, the studies were not interested on the tree inception but rather to the development of streamers, the same occurring, for example, in silicone oil. Nevertheless, these streamers may have some feature in common with the tree inception development. Under pulse voltage, the silicone gel showed two different streamer behaviors: the fast and the slow streamers. These last present an oblong bubble shape and their development time is in the range of some ms. Slow streamers are described as the only streamers present at the lower voltages. Moreover, in negative pulse voltage, only slow streamers have been recorded.

Fast streamers are called also filamentary streamers due to their shape. They growth in less than 1 μ s and reach a considerable length at a velocity higher than 3 km/s. These streamers are detected only with positive pulses and at voltages higher than the one required to have the slow streamer inception as described in Figure III-10.

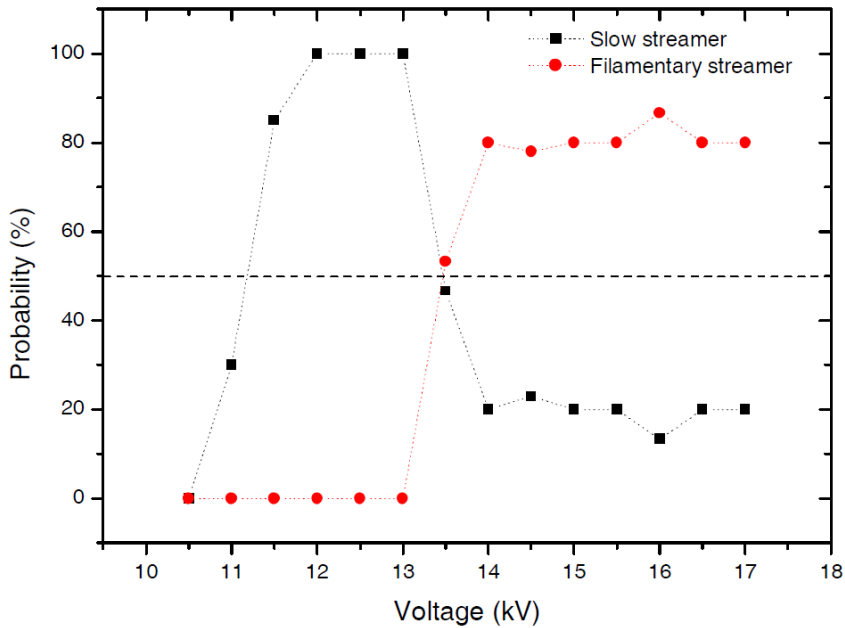


Figure III-10: Streamer inception probability versus voltage with the positive point, thanks to [71]

Another important evaluation from the researchers which considered silicone gel as a liquid dielectric is the comparison with silicone oil. Indeed, the filamentary streamer mechanism is reported also for silicone oil and many other liquid media with a similar behavior [72], [73]. On the other hand, slow streamers are common in very viscous liquids [71]. This last consideration is important to realize that slow streamers are more related to the viscosity of the material and, thus, can be a peculiar feature characterizing gels.

A second series of experiments [74]–[77] applied a highly divergent electric field to silicone gel specimens through a needle, in an experimental configuration similar to the one of the work already cited [8], [18], [70], [71]. However, in this case, the authors studied the silicone gel as a solid dielectric, thus they applied sinusoidal voltage and let it form the trees, analyzing the tree growth and shape. The tree developed through bubbles and hollow channels growing its branches both from the bubbles or from the channels with a different growing ratio [74].

Moreover, the growth rate reported was oscillating and showed a significant correlation with the voltage frequency, which may connect the three growth with the voltage phase.

The work of Salvatierra et al. [77] produces a complete analysis of the electrical tree behavior in silicone gel varying the compounds ratio. The most interesting conclusions to be highlighted regard the different state of the material due to the different compounds ratio: the silicone polymer was manufactured as liquid, gel or, elastomer. Their investigation reported two different self-healing process. Even though their physical mechanisms were not explained, the authors understood that these are characterized by two time constants. The first, having a shorter time constant, is active during the electrical degradation and reduces the tree growth closing the hollow channels. This first was detected only in gel and liquid, while the second, requiring a longer time, was partially detected also in the solid elastomer after the voltage was turned off. Moreover, some dimensional features of the tree development, such as the tree vertical growth speed, the streamer speed or the bubble characteristics were discussed in function of the silicone gel composition.

Since in this thesis examinations were employed the same silicone gel adopted in the work of Salvatierra et al., more relevant discussions and conclusions about their results will be found in the next chapters (see chapter VII-2).

IV SAMPLE PRODUCTION AND EXPERIMENTAL SETUP

IV-1 SAMPLE MANUFACTURING

Electrical treeing requires an intense divergent electric field. Different electrode configurations have been employed in literature to force the electrical tree initiation and growth inside dielectric materials with the aim to analyze the phenomenon [78]–[82].

The needle-plane configuration is the most common and the one able to realize the higher field in a single point, making the tree initiation position perfectly predictable. The theoretical maximum field at the needle tip is approximated with the Mason's equation [83]:

$$E_t = V \frac{2}{\ln\left(4\frac{d}{r}+1\right)r} \quad (1)$$

where d is the gap between the needle and the ground electrode, r is the tip radius and V is the voltage applied. Therefore, the electric field can easily reach values two or three order of magnitude greater than in the plane-plane configuration.

Each specimen employed in this work consists of silicone gel inside its sample cell: a tungsten Ogura needle, used as high voltage electrode, is immersed in silicone gel inside a manually manufactured container, made by polystyrene walls and a copper plate on the bottom, which acts as ground electrode.

The sample production procedure requires an elevated accuracy in order to minimize geometrical errors and impurity inclusions.

Each sample cell is used for a single silicone gel casting and it is composed of two parts: the container, with the ground electrode, and the top, with the high voltage electrode. The first operation consists in the containers preparation. A commercially available spectrophotometer cuvette is cut and the lower part is removed, obtaining a parallelepiped with four transparent rectangular sides while the top and the bottom are opened. In order to form a close receptacle, the ground electrode is fixed to one open side of the parallelepiped. It is made by conductive copper tape, carefully glued and shaped with a cutter. The resulting container has a square copper base of 1 cm^2 and it is 2.5 cm high. After this operation, the container is kept overturned in a clean shelf, until the silicone gel casting, avoiding any possible dust deposition.

The needle tip must be placed at a constant distance in each sample, therefore, the second preparatory operation interests the high voltage electrode setting in the top part of the sample cell. In this work the gap between the needle tip and the ground electrode employed, d , is 3 mm in all the samples. In order to hold the needle hanging in the correct position into the silicone gel, it is glued to a piece of veroboard of about 1 cm^2 through a rapid adhesive epoxy. The needle is previously cleaned with acetone. During the gluing operation, it is kept in vertical position, with the tip upward in order to prevent any possible hit which may modify its radius, ensuring the desired distance between the tip and the veroboard.

Eventually, the two parts of the sample cell are glued together through the rapid adhesive epoxy, but this operation is carried out only after the silicone gel is poured inside the container. In Figure IV-1, it is possible to see a complete sample (on the left) and the different sample cell components separately.



Figure IV-1: complete specimen (left) and sample cell components (right)

The silicone gel employed in this work is a two compound transparent silicone dielectric gel, supplied by RS Components Ltd, UK. The two liquids, labeled as part A and part B, would require to be mixed with a 1:1 ratio in order to obtain the correct degree of crosslinking. Actually, different ratios of the two compounds produce different degree of crosslinking, obtaining liquid, gel or solid products [76].

The mechanical characterization of the material for different percentage of part A compound performed by Kovalevski et al. highlights this three possible state of crosslinking. These tests were performed for different part A percentages, in mixtures cured in-situ in a rheometer isothermally at 65 °C for 4 hours.

For the lower percentage of part A compound, the resulting mixture is in liquid phase. The viscosity increases for mixtures having more than 20% part A. With 45% part A, the material reaches the first gel point. From this point up to 60% part A, the elastic modulus is low enough for the material to behave as a sticky gel-like compound. The commercially advised ratio 1:1 is almost in the middle of this range and ensure a stable gel-like state. The mixtures in the range from 66% part A to 75% part A behave like elastomeric rubber. The samples in these last A percentage range show a decrease in the elastic shear modulus, which can be

associated with an excess of part A compared to part B, and therefore with a drop of the curing efficiency. The resulting mixtures with part A ranging between 80% and 90% show a similar behavior to the samples in the first gel region, and they constitute a second gel region. Therefore, a new gel point should be expected at about 90% part A. Above this percentage the mixture is in liquid state. Figure IV-2 shows the described material behavior.

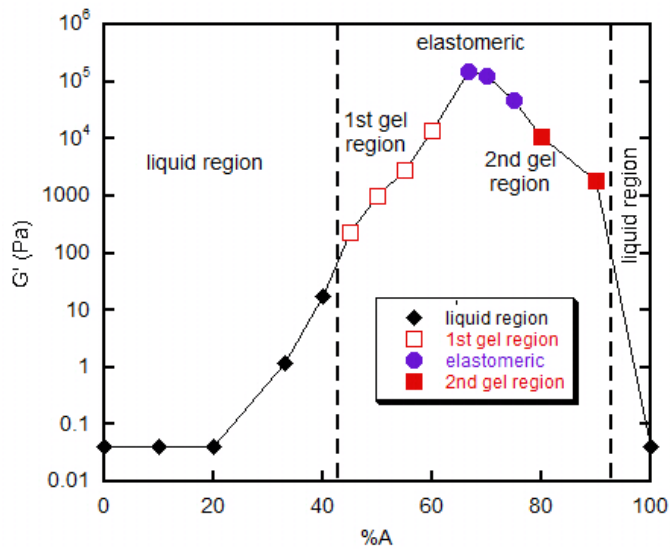


Figure IV-2: Final microstructure of samples, as the elastic shear modulus (G') against the percentage of part A (%A) [76]

In this work, two mixing ratios were used:

- 1:1 to obtain commercial silicone gel
- 7:3 to realize an elastomer

The aim of this choice is to compare the behavior of the electrical treeing in the silicone gel, which shows semi-liquid features and self-healing properties, with a solid material chemically similar, in order to assess the peculiarity of the gel state.

The following mixing and curing procedures were used for both the gel and the elastomer samples. First, the two compound are separately weighted inside a

beaker and mixed together with a constant stirring for about 5 minutes. Second, the mixture is degassed under vacuum while the continuous stirring is kept. Subsequently, the product, completely free of bubbles, is poured into the sample cells. The sample cells are quickly sealed with the rapid epoxy and set in oven at 65 °C for 4 hours to let the curing process take place and finally, the samples are left to cool down slowly overnight.

After the manufacturing, all the samples were maintained in a dry and close environment, in order to avoid, as much as possible, humidity and aging phenomena.

IV-2 EXPERIMENTAL SETUP

The measurement setups and the type of tests performed in the work are described in this chapter and are the results of several improvements. In particular, the choice of some experimental parameters, such as the voltage values and the voltage ramps, come from several preliminary tests.

IV-2.1 Measurement cell and Instruments

The measurement system was designed aiming to have a good online optical detection of the electrical tree inception and evolution during the voltage application. A scheme of the system is present in Figure IV-3. During the measurements, the specimen is set into the test cell and surrounded by silicone oil, in order to prevent discharges. The test cell is made by Polymethylmethacrylate (PMMA) with a glass window. In fact, even if PMMA is transparent, the optical quality of the images passing through the cell would not be high enough, as using glass. The test cell has an aluminum bottom connected to ground and it is back illuminated during the experiments.

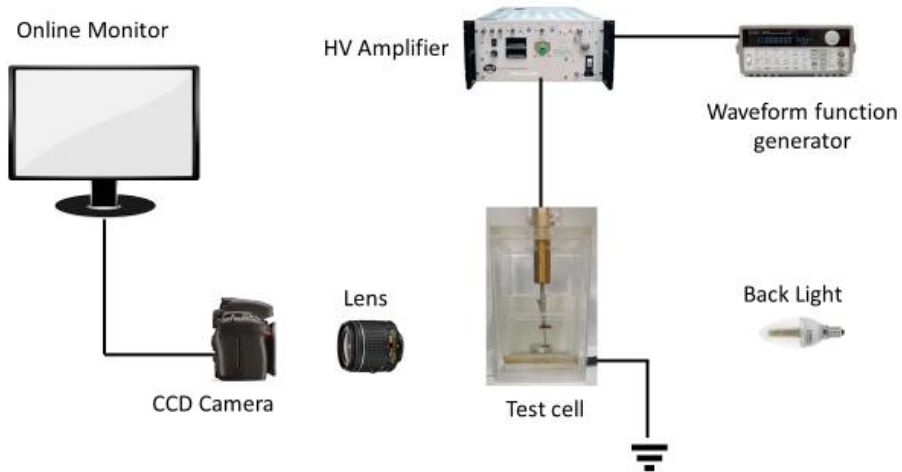


Figure IV-3: Experimental setup scheme

The upper part of the cell ends with a brass bar, connected to the sample inside the cell and to the HV generator outside.

Two HV generators were employed in the measurements:

- A high voltage amplifier from TREK Inc. model 20-20C-HS
- An experimental square voltage generator, HSR-SWG

The TREK amplifier was used to produce sinusoidal voltage and square voltage with a maximum slew rate of $250 \text{ V}/\mu\text{s}$ and it was controlled externally by a digital waveform function generator. The High Slew Rate Square Wave Generator (HSR-SWG) is an experimental square voltage generator manufactured during this thesis work. It can be summarized as a two polarity DC voltage generator connected to a MOSFET switcher supplied by Behlke, Germany. This instrument is able to produce a square voltage with short rise and fall time, in the range of hundreds of nanoseconds, up to a frequency of 2 kHz and a maximum voltage of $15 \text{ kV}_{\text{pk}}$. In this configuration, the digital waveform function generator was used only to regulate the voltage rise during the tests. The HSR-SWG was employed to produce square voltage with a $12.5 \text{ kV}/\mu\text{s}$ slew rate.

The last element of the HV control of the setup is a digital oscilloscope, which was employed in each test in order to double-check the voltage and the waveform shape.

The optical images of the sample and the tree evolution are acquired by a CMOS full high definition camera, Nikon 3100. In order to obtain a sufficient magnification, an unusual configuration is adopted: the camera lens is removed from its original location, leaving the camera with no objective, and placed at a certain distance in inverse position. It is the same principle of the reverse lens photography, commonly used to obtain cheap macro camera lens. In this way, the focal length became the distance required between the sample and the camera lens, in order to focus on the specimen, while the distance between the camera and the lens make possible the regulation of the magnification.

IV-2.2 Test procedure

The experiments carried out and described in this work can be divided into two main investigations:

- Tree inception tests;
- Tree growth evaluation and breakdown.

As already explained in the previous chapter, the tree initiation is extremely relevant for the tree analysis itself. The aim of this first typology of experiments was to evaluate the influence of different waveforms on the phenomenon. Moreover, the results obtained by these tests have brought to a model which tries to explain the physics leading the tree inception in silicone gel (see chapter VI-5). Tree inception tests were carried out for different frequencies, ranging from 1 Hz to 1 kHz and voltage waveforms:

- Sinusoidal;
- Square bipolar 250 V/ μ s slew rate;
- Square bipolar 12.5 kV/ μ s slew rate;
- Square unipolar 250 V/ μ s slew rate.

The experiments were carried out with the objective to evaluate the tree inception voltage (TIV) for the selected combinations of waveform shape and frequency. The TIV recorded is equal to the peak voltage of the waveform applied to the sample when the tree begins and it was measured increasing step by step the voltage applied up to tree initiation.

These tests took advantage of the self-healing property of the silicone gel to achieve statistically accurate results. In this material, in fact, multiple TIV measurements were carried out on the same sample when feasible. The tree inception, indeed, creates a little bubble inside the gel, close to the needle tip, which is a damage for the insulating material. Because of the silicone gel self-healing feature, when the voltage is quickly turned off after the tree detection, the bubble is usually completely closed. This behavior is likely due both to the natural inclination of gel to recover its original shape and to the presence of a liquid phase, which fill the void and merge the surfaces. Thanks to this, it was possible, not only to obtain a significant volume of data with an acceptable number of samples, but also to perform a more direct comparison between the different waveforms, using the same sample. Multiple TIV measurements were obviously not possible in the elastomer, since its solid nature does not permit self-healing.

The test procedure for the TIV was arranged after preliminary measurements and strictly followed in all the results reported in the following. In the procedure, the test starts applying the voltage from a minimum value, which depends on the needle tip radius, and increasing the voltage value with $200 \text{ kV}_{\text{pk-pk}}$ step per second until the inception is observed or until a maximum value of $14 \text{ kV}_{\text{pk}}$ for the bipolar waveforms, $20 \text{ kV}_{\text{pk-pk}}$ for the unipolar waveforms. A maximum value has been fixed to avoid a possible total breakdown of the sample or an inception with a wide damage inside the gel. In fact, after each inception, the sample must rest to recover the damage, but this is possible only if the damage is limited. Again, it is crucial to turn off the voltage quickly when the tree starts.

The TIV multiple-tests start from the lower frequency to the higher and alternate the waveforms under investigation during the frequency increment, when two of them are tested within the same sample. This choice is mainly due because the

higher is the frequency, the faster and the greater is the damage in the sample after the inception and the longer is the time required to recover it. Therefore, the probability to influence the following TIV measurement is lower starting from the lower frequency. Anyway, when the damage produced is accidentally too vast to be recovered by the self-healing properties, the sample must be discarded and therefore all the measurements previously performed are not taken into account in the data analysis.

The second evaluation assess the role of frequency and voltage waveform in the tree generation and growth. The waveforms employed in this analysis are the same used in the TIV ones. The tree growth test consists in the application of a fixed voltage to the sample and the acquisition of the optical images of the tree during time. When this fixed voltage is above the TIV, which depends by waveform and frequency, the tree starts immediately. Otherwise, the tree is initiated first using a different voltage waveform or frequency with lower TIV. After the tree is incepted, the waveform selected for investigation is applied to the sample to measure tree growth. If this procedure is followed, as soon as the tree is incepted, the waveform is switched to prevent excessive damage coming from the tree initiation stage. This procedure permits to compare the time employed to breakdown the sample for the different voltage configuration.

These tests are destructive, thus, each sample can be tested for a single couple waveform-frequency. Therefore, less combination were investigated compared with TIV tests.

The maximum duration of a tree growth test is two hours. If the complete breakdown does not occur within two hours, the test is stopped and the maximum length reached by the tree branches during the test is recorded.

From the images and the video acquired through these tests, several considerations can be stated on the electrical treeing degradation and its riskiness under different operating conditions.

V TREE INCEPTION TESTS

V-1 INCEPTION IN SILICONE GEL

The TIV tests (see Chapter IV-2.2) were carried out to assess the correlation between the voltage waveform and the electrical tree inception. In silicone gel, these tests were performed with multiple measurements on the same sample as described in chapter IV-2.2. The data obtained in these tests were elaborated and are presented in this chapter. The results shown are obtained with a statistical analysis of measurement carried out on different samples and the 95% confidence intervals presented in the graphs are based on the t-Student probability distribution.

The chance to use the same specimen for several measurements permitted to compare the behavior of two waveforms at different frequencies within the same sample. In this way, possible errors due to geometrical tolerance in the sample cell or the needle tip radius can be limited in the result analysis.

To minimize the differences due to the aforementioned geometrical tolerance between the samples and to highlight the effective trend of the inception voltage in function of the voltage applied, the data were normalized as follow. The TIV values recorded for each couple frequency-waveform obtained in a single sample and measured in kV_{pk} were divided for the average of all the TIV values obtained considering all the frequency-waveform couples measured within the sample. The

resulting values, called TIV normalized, TIVn, are dimensionless. Within each sample, the TIV trend and TIVn trend are exactly the same, since:

$$\text{TIVn}_{f,w,s} = \frac{\text{TIV}_{f,w,s}}{\overline{\text{TIV}}_s} \quad (1)$$

where $\text{TIV}_{f,w,s}$ represent a single TIV measurement carried out on sample s , at frequency f and with the voltage waveform w , $\text{TIVn}_{f,w,s}$ the value of TIVn for the same couple frequency-waveform on the same sample, and $\overline{\text{TIV}}_s$ is the average of the measurements on the sample s . Thus, TIVn and TIV simply differs by a constant.

The benefit of using TIVn instead of TIV takes place when the values obtained in different samples are related:

$$\text{TIVn}_{f,w} = \frac{1}{n} \sum_{s=1}^n \text{TIVn}_{f,w,s} \quad (2)$$

where n is the number of samples. $\overline{\text{TIV}}_s$ value is different in each sample but this is mostly due to the intrinsic differences between the radiuses of the specimen needles themselves. Indeed, even sub-micrometric differences in the needle tip can lead to significant differences in the field as shown in Figure V-1. Therefore, the $\text{TIVn}_{f,w}$ values is the most appropriate quantities to highlight the trend of the tree inception due to frequency and voltage waveform avoiding to take into account the bias due to the geometrical tolerance among the samples.

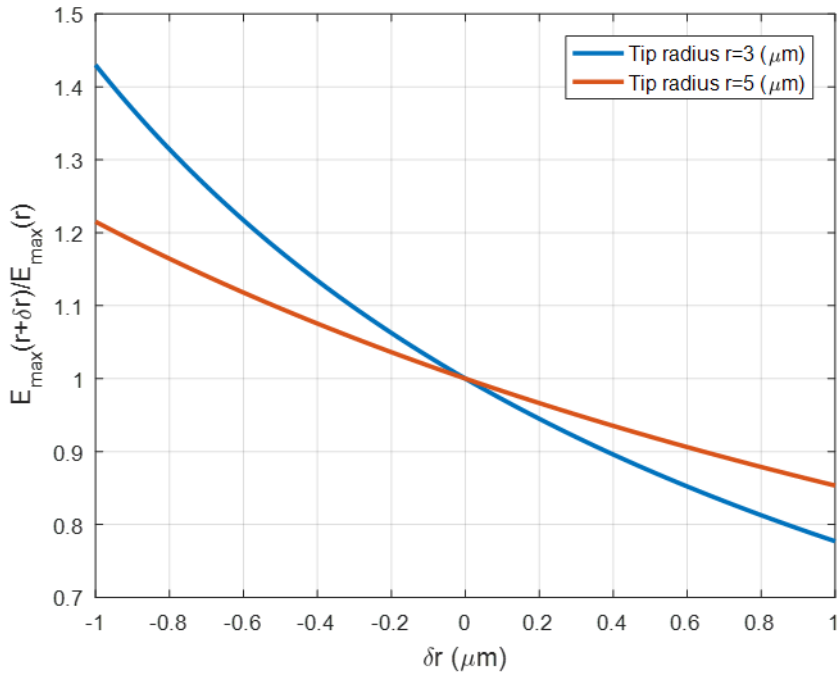


Figure V-1: Effect of needle tolerance on peak voltage at needle tip

This simple data analysis method is applicable since it does not distort the nature of the results and their statistic value. In Figure V-2, it is possible to compare the TIV and TIVn at 10 Hz for sinusoidal and square waveform (250 V/ μs slew rate). Both the values can be displayed on Weibull chart with a good correlation, meaning that the Weibull distribution is appropriate for the phenomenon analysis. Moreover, the β shape parameters are quite high in the TIV chart, 5.6 for the square and 9 for the sinusoidal waveform, and they are also higher in the TIVn one, 9 for the square and 15.2 for the sinusoidal waveform. This implies that data display a low statistical dispersion.

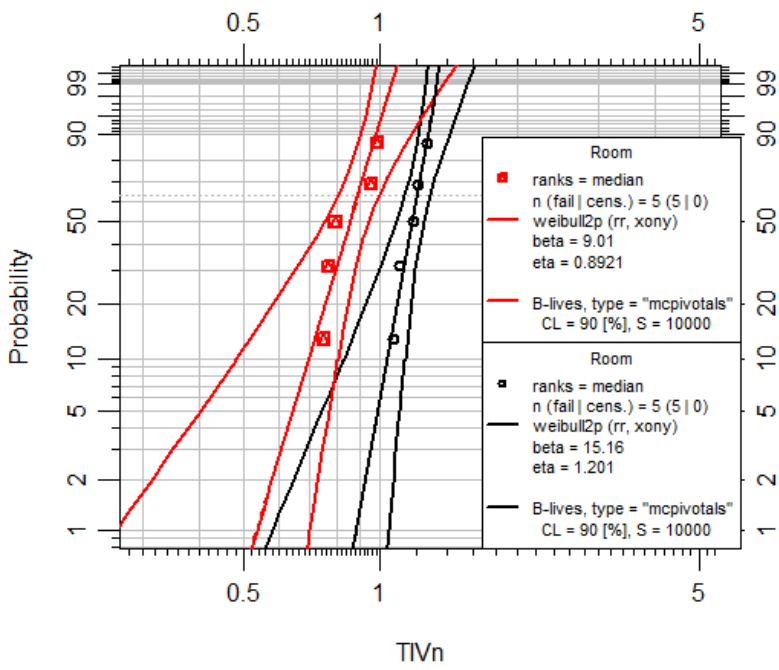
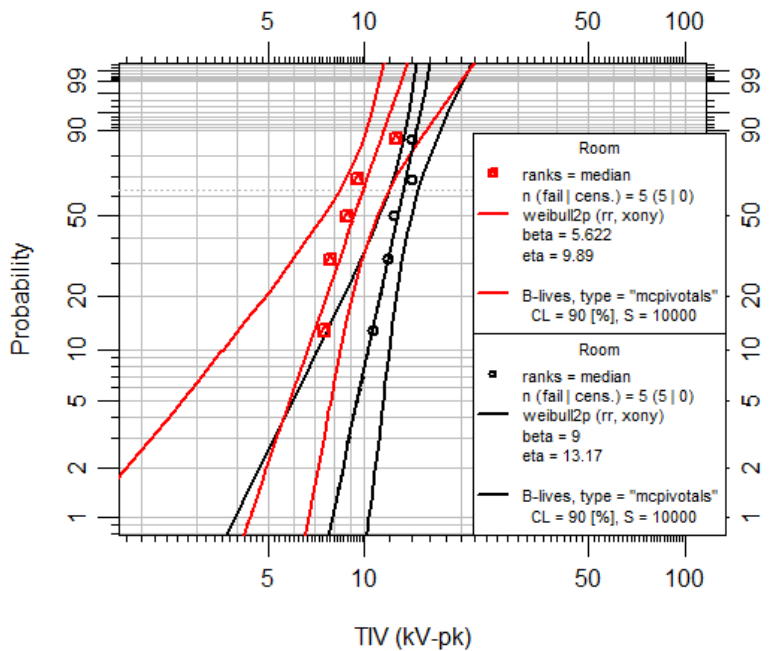


Figure V-2: Weibull chart of the results at 10 Hz of TIV (up) and TIVn (down) for sinusoidal (black) and square waveform (red)

Some tests reached the maximum voltage value employed in the TIV experiments, 14 kV_{pk} for the double polarity, 20 kV_{pk} for the single polarity, without any inception. In these cases, the value reported for the data elaboration was set equal to the maximum voltage applied and the data were censored to estimate the Weibull scale and shape parameters as well as the confidence intervals.

Part of the preliminary investigation focused on the evaluation of a possible memory effect in a sequence of measurements on the same sample and on the rest time required between two measurements. Indeed, using the same frequency-waveform couple, inspecting the TIV values in a series of repeated measurements did not provide evidence of a trend in the data. Thus, the sample did not degrade appreciably after several measurements and the TIV value recorded was almost equal to the one obtained in the first test in the fresh sample. Therefore, the multiple TIV tests were considered reliable to evaluate the inception phenomenon.

A confirmation of this behavior can be found in Table 1, which shows an average of the results obtained on five samples at 1 Hz. The first measurements, carried out on fresh samples, had results similar to the ones obtained after the whole series of TIV tests.

	FIRST MEASUREMENTS [KV _{PK}]	LAST MEASUREMENTS [KV _{PK}]
SINUSOIDAL	13.7 ± 1.9	13.8 ± 1.6
SQUARE	8.2 ± 1.6	8.5 ± 1.4

Table 1: TIV measured on fresh samples (first measurements) or after a series of tests (last measurements). Average on 5 samples

V-1.1 Sinusoidal and Square Comparison

Qualification and diagnostic evaluation in industrial application are often performed employing sinusoidal waveforms, which are easy to obtain using transformers and are characterized by low noise levels. However, in practical applications, the insulating material can be subjected to different electrical stress, such as in power modules application (see chapter II-2). Therefore, the first evaluation of this work focused on possible difference between square and sinusoidal waveform regarding tree inception.

Complete series of multiple TIV measurement testing on each sample the sinusoidal and square voltage with frequencies ranging from 1 Hz to 1 kHz were carried out on 5 silicone gel specimens. The tip radius of these first samples was 5 μm . The measurement elaboration is shown in Figure V-3.

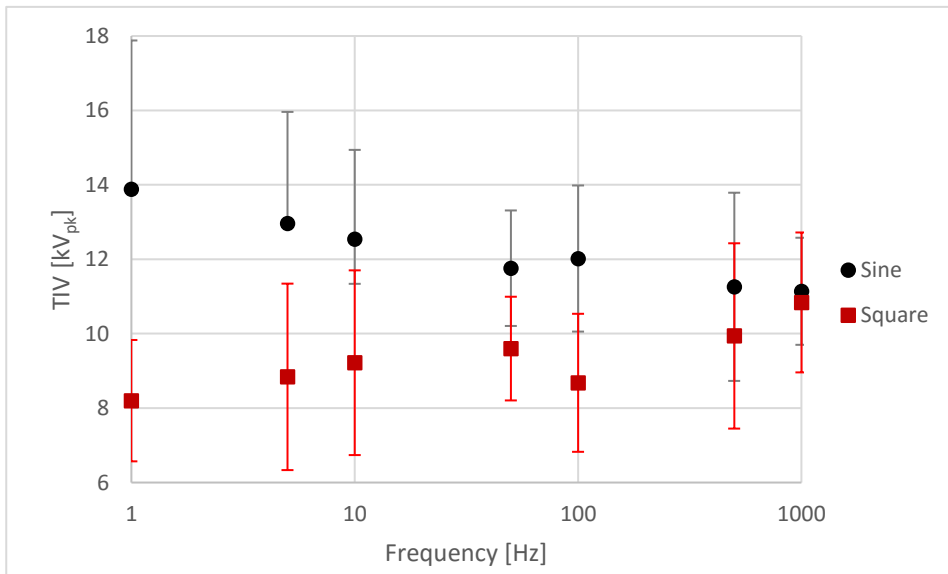


Figure V-3: Average TIV for 5 μm tip needle samples

The $\overline{\text{TIV}}_s$ of each sample ranged from 9.8 kV_{pk} to 12.7 kV_{pk} and the global average of all the measurements is 10.8 kV_{pk}.

Considering the variability of the phenomenon and the possible sources of geometrical errors, the variance is not really wide, thus the samples were properly manufactured. A test issue should be highlighted: some measurements reached 14 kV_{pk}, without the inception and this is the reason of the unbalanced confidence intervals for the lower frequencies of the sinusoidal waveform.

Despite the reliability of the sample manufacturing process, for a more accurate analysis of the tree inception, the TIVn trends were calculated and shown in Figure V-4.

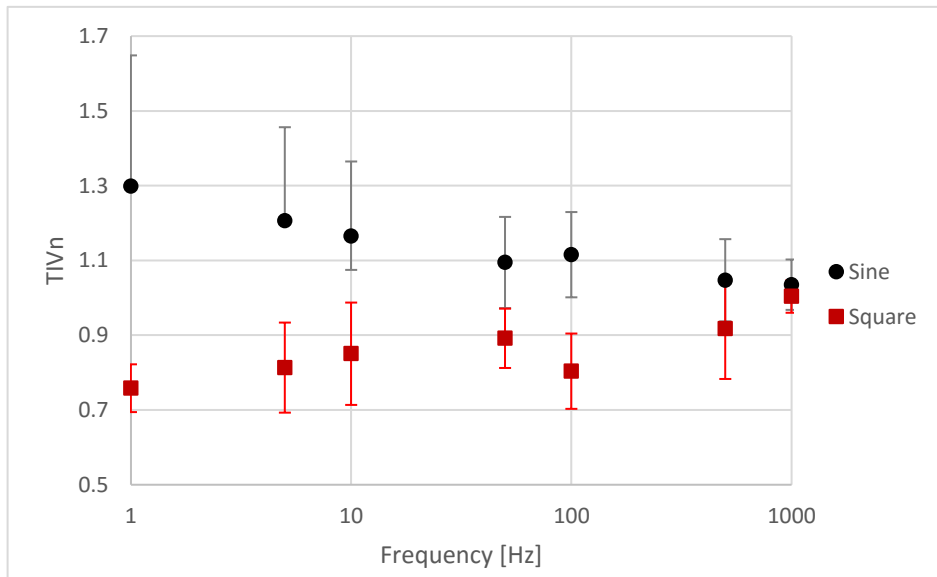


Figure V-4: Average TIVn for 5µm tip needle samples

The trend of the data presented in Figure V-4 does not differ significantly from the ones in Figure V-3, confirming that TIVn can be used instead of TIV. Nevertheless, the data in Figure V-4 better underline the inception behavior since the distance between the two curves at the lower frequencies is wider and the confidence intervals are significantly lower. This last means that the differences between the measurements obtained in each sample are reduced considering the

TIVn instead of the TIV, thus, the general trend can be considered a good approximation of the trend in each sample.

TIV behavior in function of the frequency is opposite between sinusoidal and square voltage: higher frequencies reduce the TIV using sinusoidal waveforms while using square voltages the TIV increases. In order to confirm this trend, the comparison between sinusoidal and square voltage waveforms was replicated employing specimens with 3 μm tip radius needle.

The results obtained are presented in Figure V-5.

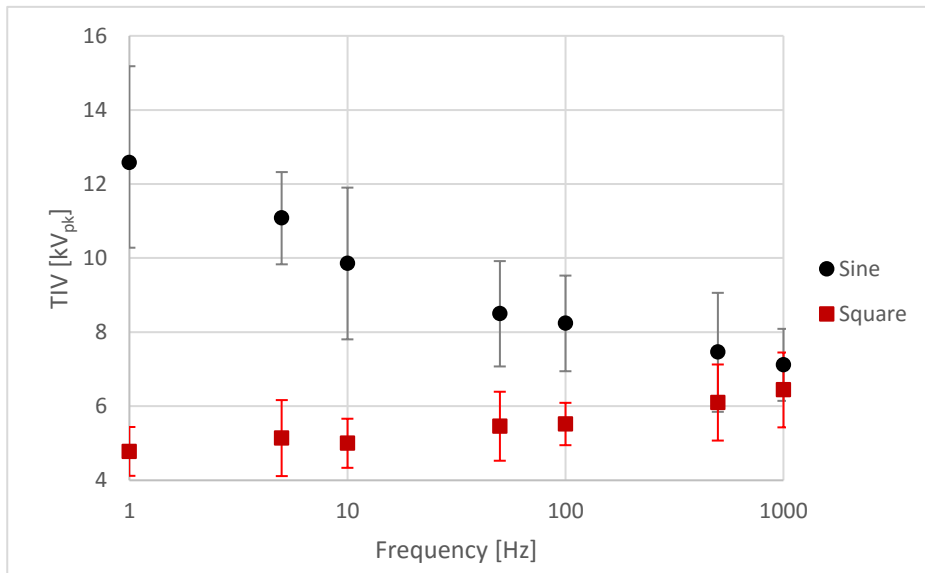


Figure V-5: Average TIV for 3 μm tip needle samples

In this case, the global average value of the TIV was 7.40 kV_{pk}, while \overline{TIV}_S ranged from 6.43 kV_{pk} to 8.63 kV_{pk}. In this case also, the TIVn values were calculated and the resulting data are shown in Figure V-6.

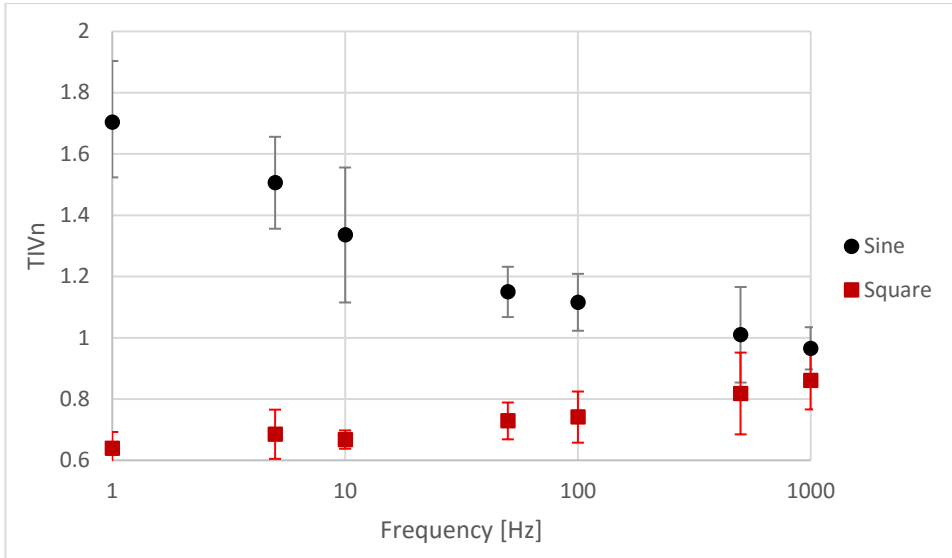


Figure V-6: Average TIVn for 3µm tip needle samples

The results obtained with the smaller needle tips confirm the trend: the TIV increment for the square voltage is comparable to the one previously reported, while the decrease in the sinusoidal voltage is even wider. This is partially due to the limit on the maximum voltage applied, which limited the values obtained in Figure V-4 for the lower frequencies in sinusoidal voltage. Therefore, these last results are more accurate, especially for the lower frequencies, in order to better understand the inception phenomenon.

This peculiar trend with the frequency is quite unexpected. In fact, in solid materials, the electrical tree inception is related to the number of polarity reversals, and the TIV decreases significantly with the frequency. This is not true in the results obtained here for the gel. Therefore, it is reasonable to believe that the inception in gel should be modeled with some peculiarities, taking into account its similarity with liquids.

V-1.2 High slew rate

In the results shown in the previous paragraph, a remarkable difference exists between sinusoidal and square waveform TIV for the lower frequencies. Since the time when the sample is subjected to the maximum voltage is longer for the square wave, it could be concluded that this time is a key parameter for the phenomenon. Indeed, testing the specimens with a “cosrect” waveform (see Figure V-7) rejected this hypothesis. The applied “cosrect” waveform had the rise time similar to the 1 Hz sinusoidal voltage and the width equal to that of the 1 Hz square voltage. Under this waveform, tree inception was not observed up to 14 kVpk. This result is comparable with that of the 1 Hz sinusoidal waveform. Therefore, the most significant parameter for tree inception in silicone gel should be the voltage slew rate.

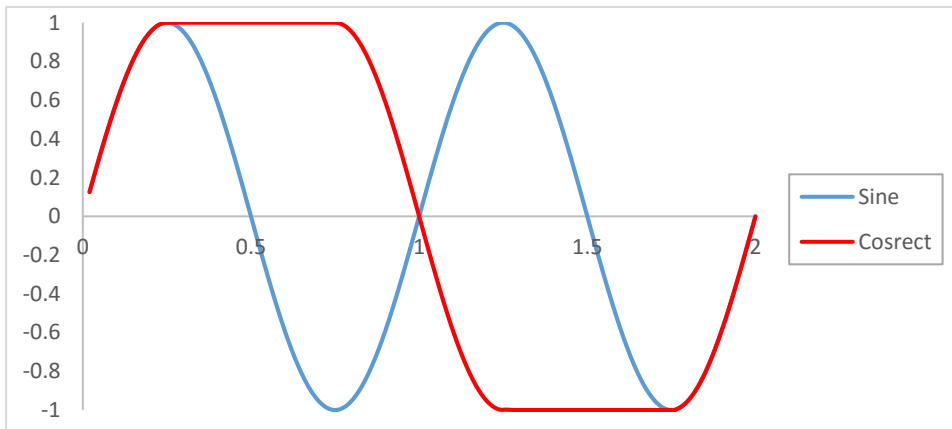


Figure V-7: example of cosrect waveform

In order to assess the influence of a shorter rise time in the tree inception, the HSR-SWG was employed. The tests were performed on samples with 5 μm needle tip radius. The data shown in Figure V-8 are obtained averaging 5 samples and compare the results obtained with the square voltage with 250 $\text{V}/\mu\text{s}$ slew rate and the one with 12.5 $\text{kV}/\mu\text{s}$ slew rate produced through the HSR-SWG.

The confidence intervals are not shown since they would overlap in several points. Moreover, due to the limited amount of samples, the confidence intervals are too large to appreciate completely the small differences. Nevertheless, the average values reported with the higher slew rate tests are always lower than the ones obtained with the 250 V/ μ s slew rate (except for the 100 Hz values, where they are barely the same, probably due to an inaccurate value obtained at 250 V/ μ s, since this is also unaligned with the general trend of the other values). Therefore, it is possible to conclude that this slew rate increase of about 50 times, between 250 V/ μ s and 12.5 kV/ μ s, decreases the values of TIV of about 13% on average and, thus, that the slew rate is an important parameter in the inception phenomenon.

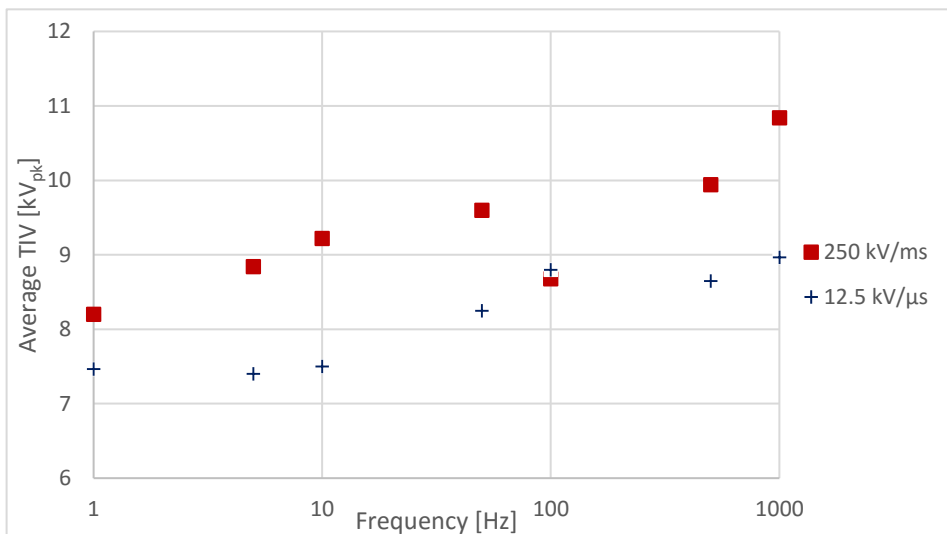


Figure V-8: TIV comparison between square voltage with 250 V/ μ s and 12.5 kV/ μ s slew rate

V-1.3 Unipolar Square Voltage

In many of its electrical applications, silicone gel is subjected to unipolar square waveforms, e.g. in a large part of the power module components. Thus, the TIV has been investigated under these conditions. Moreover, the possibility to

analyze a single polarity permits to assess the influence of the polarity itself on the tree initiation, improving the knowledge of physics behind the inception.

Multiple TIV tests were carried out on 5 samples alternating unipolar positive and unipolar negative square waveform, with 250 V/ μ s slew rate. The results obtained were normalized using the TIVn, following the same method employed for the comparison between square and sinusoidal waveform and explained at the beginning of this chapter in Equation V-2. Figure V-9 shows the data obtained.

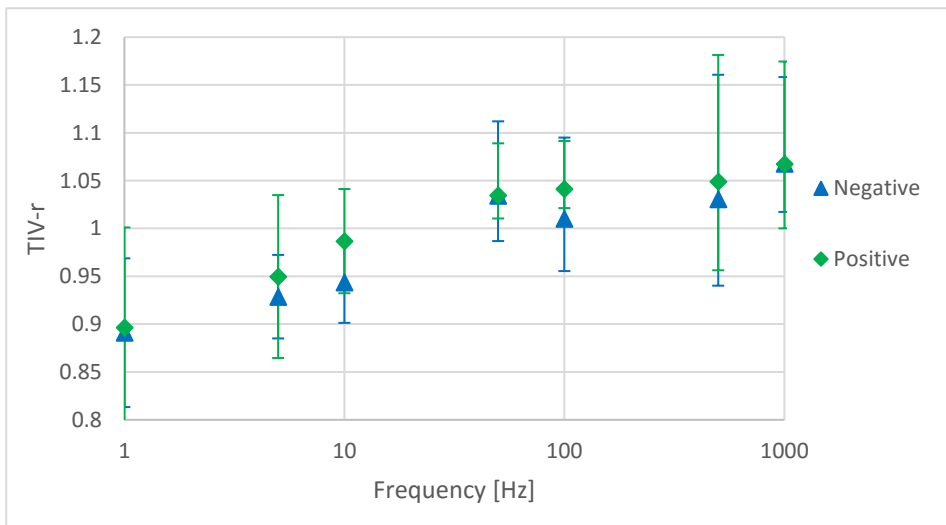


Figure V-9: TIV-r for unipolar square waveform

The measurements reached the 20 kV_{pk-pk} in few tests at the higher frequencies. Consequently, the upper confidence bounds of these frequency values are larger in these tests. Nevertheless, the TIV seems to increase slowly with frequency and a clear difference between positive and negative unipolar waveforms is not recorded. This is an interesting and unexpected result. In fact, the metal at the needle tip should have a much lower barrier for electron injection, compared with hole injection (in [84] the barrier for injection in mineral oil of electrons and holes from a stainless steel tip were estimated as 0.20 eV and 0.41 eV, respectively). Consequently, we expect that the time needed to build up a

space charge limiting field (SCLF) region is longer for positive polarities. Also, it was reported that, using lightning impulse, streamer generation in silicone gel is remarkably affected by the pulse polarity [71], being “fast streamers” incepted only under high voltage positive pulse (positive and negative polarity both present only “slow streamers” at lower voltages). Indeed, using lightning impulse, space charge is not generated prior streamer inception, and the subsequent phenomena are related to the mobility of positive and negative ions in the gel [28], therefore the streamer mechanism under pulses should differ from the one in tree inception, where the space charge injection happens. At any rate, it was reasonable to find a difference in the tree initiation. Considering the square voltage comparable to pulses, it is possible to observe that the TIV tests evaluate the lower voltages capable of making the tree starts, which are interesting for real application, and thus the initiation phenomena may be lead to the so-called “slow streamers”, since tree inception and “slow streamer” have similar shapes. Actually, it is more reasonable to distinguish pulse and square voltage inception. Therefore, in this last case, the comparable results obtained by positive and negative polarities are likely due to the very high electric field, which reaches the SCLF in both the polarities, without remarkable differences at the macroscopic level.

A second significant evaluation can be made comparing the results of the unipolar tests with the one obtained with the bipolar waveform as shown in Figure V-10. In this case, it is employed the TIV and not the TIVn, since different samples were used to obtained the data.

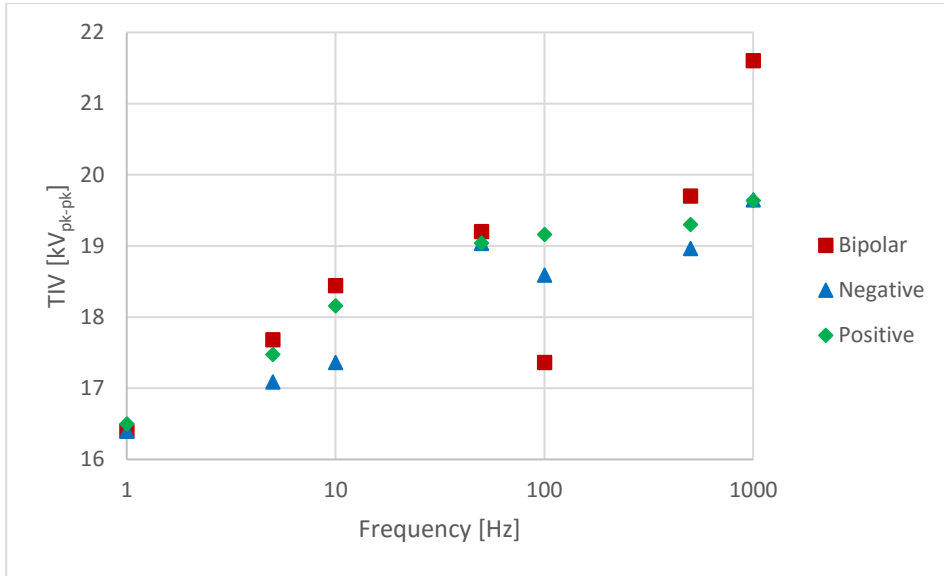


Figure V-10: TIV for unipolar and bipolar square voltage

The TIV values for the three waveforms are extremely close. In fact, not only the global trend is the same, but also the actual values can be considered equivalent (again, except for the 100 Hz square voltage value), taking into account the use of different samples and the limit value of 20 kV_{pk-pk} reached in some measurements for the unipolar voltage at the higher frequencies.

In conclusion, the tree inception mechanism is the same for the unipolar waveform and for the bipolar waveform, therefore, it is directly connected to the peak to peak voltage.

V-2 INCEPTION IN ELASTOMER

Electrical treeing in gel has peculiar features, mainly due to the self-healing property, which force to study the tree development from a new point of view. In order to support this theory, TIV tests were carried out on elastomer. Since this thesis focuses on the silicone gel study, the elastomer is used exclusively for comparison. For this reason, the material employed was made by the same

chemical compound employed for the gel, but with a different ratio A/B (as described in chapter IV-1): in this way the difference reported must depend on exclusively on the solid nature of the material.

The data shown in Figure V-11 were obtained averaging 3 samples for each point. In this case, since the material was solid, each sample was employed for a single measurement, thus it was not feasible to calculate the TIV-r and the confidence bounds are quite wide.

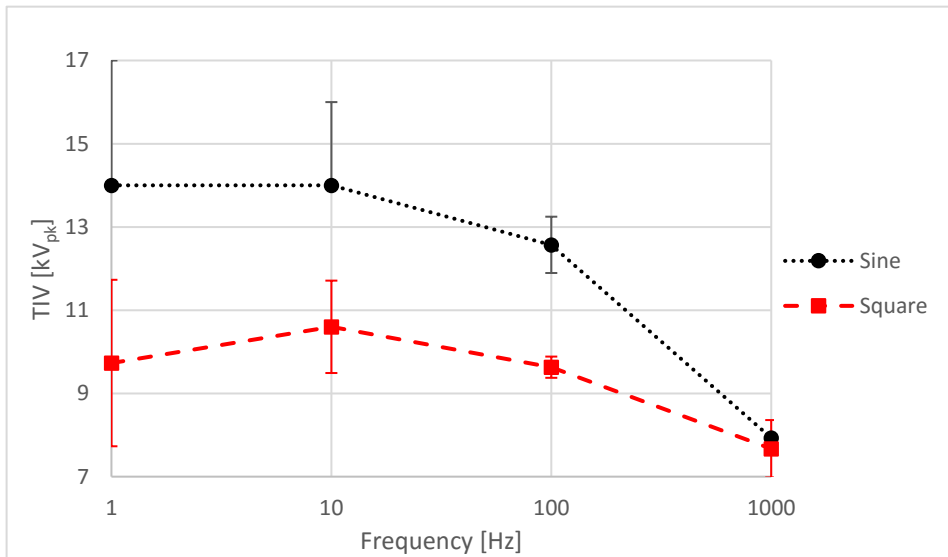


Figure V-11: TIV in elastomer

The values obtained for the lower frequencies are slightly higher than the one reached in the silicone gel for the same frequencies, the values at 100 Hz are almost the same, while at 1 kHz the TIV is lower in solid than in gel. The general trend is different to the one observed in the gel: the TIV in the solid decreases at higher frequencies; in the sinusoidal waveform, the TIV decreases with the frequency as in the gel, but it is sensibly higher in the elastomer than in the gel. Following these considerations, it is possible to conclude that the higher frequencies strongly decreases the TIV, in both square and sinusoidal voltage, thus the inception is likely linked to a frequency related phenomenon. As presented in

chapter III-2, this assertion is commonly supported by the great part of the theories and models related to the electrical tree. However, the theories cannot hold for silicone gel, due to its peculiar dependence on frequency shown above.

VI TREE INITIATION MODEL

The results shown in chapter V highlight fundamental differences between the tree inception in silicone gel and in solid materials. The trend with the frequency is the most relevant peculiarity: the small increase of the inception voltage with the frequency, in fact, invalidates the theory of a phenomenon of energy accumulation, which is the most common assumption for solids (see chapter III-2.2). Therefore, in this chapter, it will be proposed a model of tree inception in silicone gel which can be related to a single event instead of a long energy accumulation. A complete model of this phenomenon should include the contribution of two features to be evaluated together: the charge injection and extraction mechanism, and the way that this charge produce the damage resulting in the formation of an electrical tree.

VI-1 SPACE CHARGE INJECTION

A brief introduction on the electrical tree inception and on the other tree stages is proposed in chapter III-2.2. As previously explained, the inception is the first stage of an electrical tree and, contrarily to the other stages, it is still unclear.

Complete studies on electrical treeing have been carried only on solid material until now. A common opinion on electrical tree inception in AC voltage is that the phenomenon is related to the charge carrier movement in the inception area. In particular, the charge injection and the charge recombination are the two phenomena, which are recognized to be the fundamental of the inception process [85], [86]. Indeed, the charge recombination may be the cause of Joule heating

and thus it can provoke the damage which, following a series of chemical and mechanical degradation, can create a void [87]. Other researchers concluded that the space charge may lead to an enhancement of the local electric field, which exceeds the breakdown threshold [88], [89]. In general, the stress due to the charge carriers is recognized to be the inception trigger, even if the physics of the degradation process is still under debate.

The charge injection has been measured both with direct method or by detecting the light emission [90]–[92]. Baumann et al. have suggested the existence of a field dependent electron mobility. A consequence of this hypothesis is that charge injection and extraction occur in the part of the alternating stressing cycle when the field in the dielectric close to the electrode exceeds the material dependent threshold. Moreover, they have concluded that the electroluminescence was not due to the charge recombination. Contrarily, many other authors [50], [93], [94] have suggested that injection current is due both to electrons and holes, injected alternately during each half cycle and that electroluminescence is due to the recombination of electrons and holes inside the material.

The charge injection process must be, anyway, the fundamental process to be analyzed in order to understand tree inception also in silicone gel. The charge injection through a potential barrier has been studied for many years and there are two main approximations for it [37]: Schottky-Richardson and the Fowler-Nordheim. The first one is commonly the best fitting for a low field approximation and in this injection model it is assumed that the barrier is due to the electrostatic attraction between the electrons and the metal, the latter being positively charged since the electrons have left it. Therefore, the model calculation starts from the well-known Coulomb attraction law. The Fowler-Nordheim approximation, on the contrary, is the most reliable for very high voltage application, where peculiar high field effects, such as tunneling, must be taken into account, using quantum mechanical model and wave functions. In the last decades, a third approximation has been successfully proposed for material at room temperature [95], describing the current density j as a function of the electric field, E :

$$j(E) = \alpha e^{\beta E} \quad (1)$$

where the constants α and β depend on temperature and potential barrier height and are the same for both electrons and holes. The model studied in this thesis work takes advantage of the simplicity and effectiveness of this last approximation in order to analyze the behavior of silicone gel.

VI-2 CHARGE INJECTION MODEL

The correlation between charge injection or recombination and electroluminescence is a useful physical property, which permits to validate the theories with the experimental results. The starting point of the model discussed in this thesis is the Alison et al. model [96], which uses a dynamic bipolar charge recombination model to explain the charge injection and the electroluminescence behavior experimentally recorded in a pin-plane configuration, similar to the one employed in the experimental setup used in this work. Since the electrical treeing initiation must be correlate to the space charge injection, the space charge analysis is the basis for an inception model.

The geometry of the sample is simplified as a concentric spheres electrodes arrangement. The inner electrode radius, r_0 , is set equal to the needle tip radius, while the ground electrode radius, r_2 , is equal to the distance between the needle and the ground electrode. In the model, it is assumed that the space charge is localized exclusively within a region between the inner electrode radius, r_0 and a length r_1 . The concentric sphere geometry is a totally acceptable simplification, since the axial symmetry of the electric field at the needle tip is respected, well simulating the central zone of the needle-plane electrode, which is the one of interest. Indeed, even though the real electric field is slightly different to the one obtained with this geometry (see equation IV-1), it does not influence comparative and qualitative evaluations between different waveforms, which are the aim of the model.

The calculation is carried out starting from the simplified geometry above described following a series of assumptions on the physical model:

- the space charge region is small compared with the sample, therefore: $r_1 \ll r_2$;
- space charge density, ρ , is constant between r_0 and r_1 , zero outside this region;
- transport and diffusion outside this region are neglected;
- the space charge density depends on time t through $E_0(t)$, the field at the injecting electrode.

Considering $V(t)$ the potential close to the injecting electrode, it is possible to solve the Poisson's equation obtaining:

$$E_0(t) = \frac{V(t)}{L_0} - \frac{\rho(t)}{\varepsilon_0 \varepsilon_r} K(r_0, r_1, r_2) \quad (2)$$

Where ε_0 is the permittivity of the free space and ε_r is the relative permittivity of silicone gel, which is equal to 2.8. The term L_0 is a scale length which depends on the electrode geometry and K is a function of the electrode geometry and the space charge region thickness. Both these terms have dimensions of length and, in the concentric sphere electrode arrangement, are equal to:

$$L_0(r_0, r_2) = (r_0)^2 \left(\frac{1}{r_2} - \frac{1}{r_0} \right) \quad (3)$$

$$K(r_0, r_1, r_2) = \left(\frac{r_1^3}{3} - \frac{r_1^2 r_2}{2} - \frac{r_0^3}{3} + \frac{r_0^2 r_2}{2} \right) / (r_0^2 - r_0 r_2) \quad (4)$$

The space charge density and the injection current can be easily related through the continuity equation [97]. Indeed, the charge density flowing across the surface area of the injecting electrode S into the space charge volume v increases the space charge density inside this same volume:

$$\int_S j(t) ds = \int_v \dot{\rho}(t) dv \quad (5)$$

where j is the charge injection current. At this point, differentiating Equation VI-2 with respect to time and using Equation VI-5 it is possible to obtain:

$$\dot{E}_0(t) = \frac{\dot{V}(t)}{L_0} - \frac{kj(t)}{\epsilon_0 \epsilon_r} \quad (6)$$

where the term k is a dimensionless constant which depends, as K , on the model geometry and the space charge region thickness. In the electrode arrangement used:

$$k = \frac{3r_0^2}{r_1^3 - r_0^3} \left(\frac{r_1^3}{3} - \frac{r_1^2 r_2}{2} - \frac{r_0^3}{3} + \frac{r_0^2 r_2}{2} \right) / (r_0^2 - r_0 r_2) \quad (6)$$

In order to proceed with the calculation of the space charge injected inside the material, it is required to choose a charge injection model. In this analysis, as discussed in chapter VI-1, the injection current is considered to follow Equation VI-1. The parameters α and β are set equal to the ones employed in [96], thus $1 \times 10^{-5} \text{ Am}^{-2}$ and $8 \times 10^{-8} \text{ V}^{-1}\text{m}$ respectively. The values chosen have been validated with epoxy resin, thus is likely that they are not the same for silicone gel. Nevertheless, the influence of their variations is relatively low for the charge injection and not significant at all for the global behavior.

Since the derivate of the potential at the high voltage electrode surface $\dot{V}(t)$ is known, because it is only due to the voltage waveform applied, the electric field is easy to be numerically evaluated. Moreover, the space charge injected in the proximity of the needle tip in the volume v with space charge density ρ is calculated through the integration over time of:

$$\rho(t) = j(t) \Delta t \frac{S}{v} \quad (6)$$

where Δt is the time step length employed in the calculation.

VI-3 CHARGE INJECTION CALCULATION

The numerical calculation followed the model explained in these last pages (chapter VI-2) and tried to simulate conditions as similar as possible to the ones used in the TIV measurements. In the calculation carried out, in fact, the inner electrode radius r_0 have been set equal to $5\ \mu\text{m}$ or $3\ \mu\text{m}$, following the dimensions of the needle tips employed in the experimental part. The space charge region, where the space charge density differs from zero, has been set arbitrary to $3\ \mu\text{m}$ thick, thus r_1 was $8\ \mu\text{m}$ or $6\ \mu\text{m}$ depending on r_0 . The outer radius r_2 has been set to $3\ \text{mm}$, equal to the distance between ground and high voltage.

The results of a calculation with an inner radius of $3\ \mu\text{m}$ under sinusoidal voltage at $50\ \text{Hz}$ are shown in Figure VI-1.

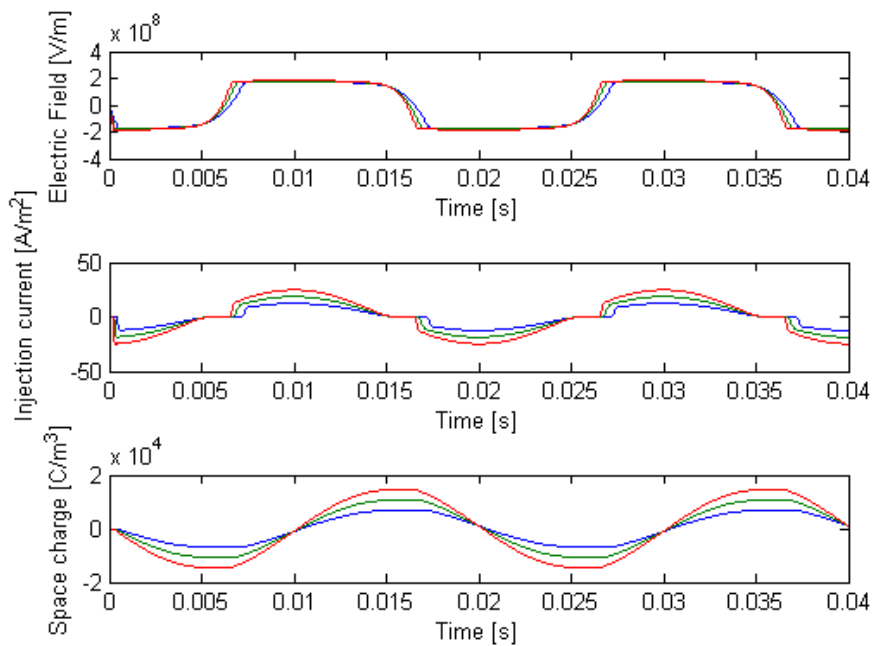


Figure VI-1: E_0 , j and ρ behavior for $50\ \text{Hz}$ sine waveform at $6\ \text{kV}_{pk}$ (blue), $9\ \text{kV}_{pk}$ (green) and $12\ \text{kV}_{pk}$ (red)

The colored curves show the values of the electric field close to the needle tip, the injection current and the space charge for the different peak voltages applied.

The results are similar to the ones obtained by Alison et al [96] with high voltage applied and thus when the SCLF was easily reached. Since the results obtained with the calculation by Alison were confirmed evaluating experimentally the electroluminescence in their samples, it is reasonable to consider highly realistic the behavior obtained also in this calculation.

Confirmed the validity of the calculations performed, the model has been implemented employing a square voltage with 250 V/ μ s slew rate. The results are shown in Figure VI-2. All the other parameters adopted in the calculation, apart the voltage waveform, are the same than in the results presented in Figure VI-1.

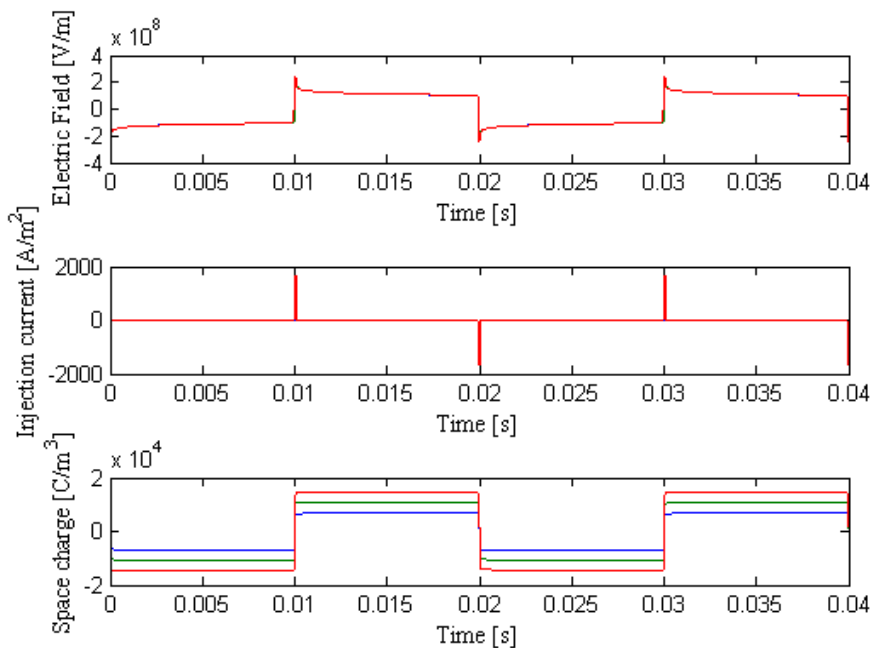


Figure VI-2: E_0 , j and ρ behavior for 50 Hz square waveform at 6 kV_{pk} (blue), 9 kV_{pk} (green) and 12 kV_{pk} (red)

It is even clear that, under square voltage, the SCLF is easily reached in this geometrical configuration: the electric field, indeed, does not show any variation increasing the peak voltage applied from 6 to 12 kV.

Therefore, it is possible to conclude that the electric field is almost independent of the voltage applied in this range of operation. This is only partially true: the only detectable variation of the electric field at the electrode consequent to an increment of the applied voltage is a change of rise time in the sinusoidal waveforms. Increasing the applied voltage indeed, these curves show a major slope of electric field curve during polarity reversals and a maximum field slightly higher.

The major parameter affecting the injection current is the derivative of the voltage, \dot{V} . In the square waveform, for example, the injection current reaches an extremely large maximum during rise and fall times, but falls to very low values when the value of \dot{V} is zero. Contrarily in the sinusoidal waveform where \dot{V} is never null (except for two instants in each period), an injection current is present during all the time and changing even when $E(t)$ saturates. This results in an injection current that continues throughout most of the ac-cycle but is orders of magnitude lower than that found in the square waveform.

Direct consequence of the injection current is the space charge stored into the material. Since the injection current happens in an extremely restricted period in the square waveform, the space charge is accumulated almost only during the polarity reversal and it remains constant when the voltage is at the peak values. In sinusoidal voltage, the space charge roughly lags the voltage by 90° but has a similar waveform because the injection current continues throughout the whole period. Despite the substantial difference in the space charge accumulation trend between sinusoidal and square voltage calculation, the maximum amount of the space charge accumulated is comparable.

The difference between sinusoidal and square voltage considering the three physical quantity analyzed is relevant, therefore it could be possible to find a direct

connection of one of these to the tree inception. In order to evaluate this possibility, the values of ρ , E_0 and j have been calculated for the two waveforms at different frequencies, the same of the experimental TIV tests. The trends are not significantly influenced by the voltage frequency. On the other hand, the actual values can vary deeply. Since no relevant variations have been observed in the trends, it becomes essential to assess the maximum values reached. These are presented in Figure VI-3, Figure VI-4 and Figure VI-5, where the values are obtained taking into account a peak voltage of 9 kV. The behaviors are quite interesting. The electric field on the surface of the silicone gel close to the needle tip reaches the higher value in the square voltage and, under this waveform, it is constant with the frequency. In sinusoidal voltage, the behavior is sensibly different: the electric field has a logarithmic increase with the frequency (in Figure VI-3 the frequency is represented in logarithmic scale), reaching a value close to the one obtained under square voltage for the higher frequencies.

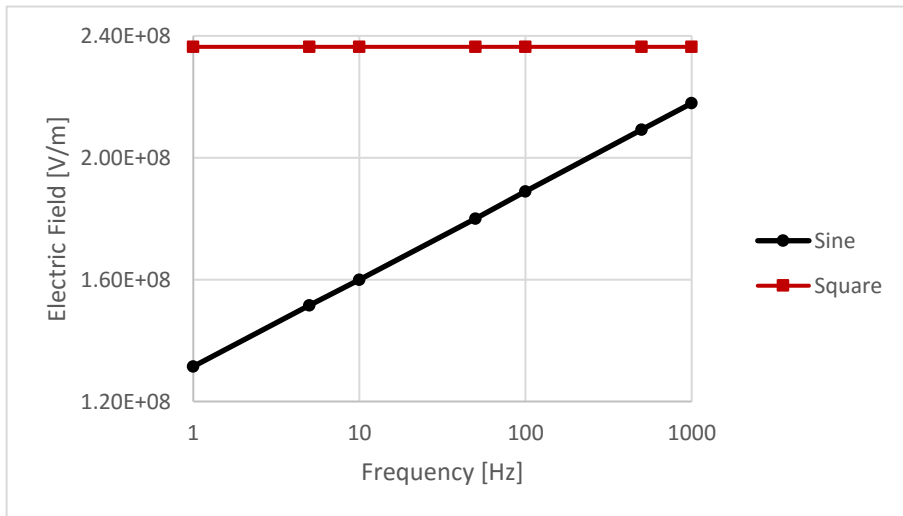


Figure VI-3: maximum values of E_0 as a function of frequency, calculated at 9 kV_{pk}

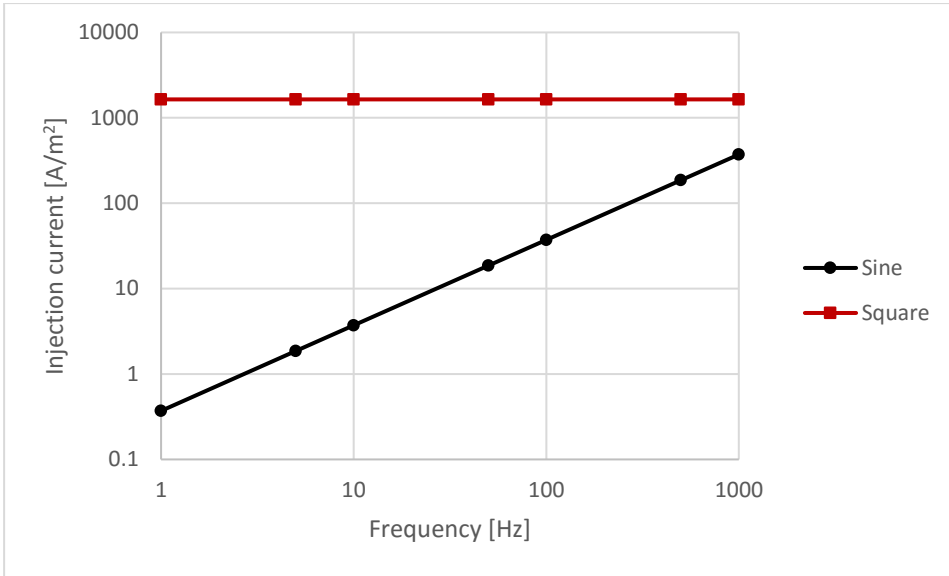


Figure VI-4: maximum values of j as a function of frequency, calculated at 9 kV_{pk}

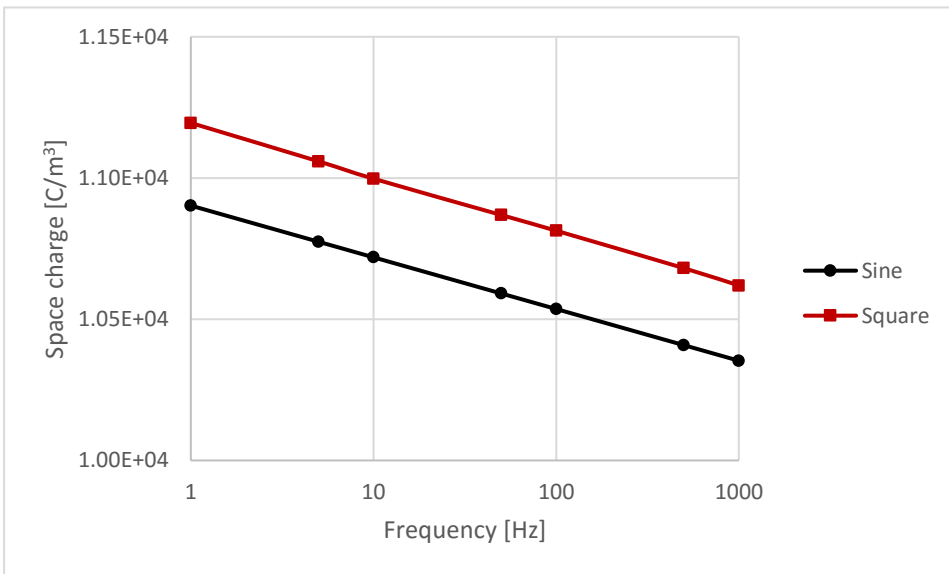


Figure VI-5: maximum values of ρ as a function of frequency, calculated at 9 kV_{pk}

The calculations performed simulating the square voltage show a second physical quantity not varying: the maximum injection current is, in fact, constant for each value of frequency. The sinusoidal voltage, instead, shows a growth of this quantity. The injection current increases proportionally to the applied frequency, therefore creating an extremely wide difference between lower and higher frequencies.

Finally, the last physical quantity investigated, the maximum space charge accumulated, shows a similar trend and similar values for both the waveforms analyzed. Despite the significant difference between sinusoidal and square voltage obtained in the other two quantities investigated, both the two space charge trends show the same slight decrease with the frequencies and a difference between the two waveforms of around the 3% of the actual value.

The analysis of the three quantities does not provide results able to connect clearly one of them to the TIV experiments and, therefore, to the tree inception. The first two, in fact, do not show any variation in function of the frequency applying the square voltage, which is not compatible with the trend obtained in the TIV for this waveform. Moreover, the linear increase of the injection current with the frequency obtained under a sinusoidal voltage is far from the TIV result trend. On the other hand, the space charge accumulated, showing the same trend for both the waveforms, contrast with the TIV experimental results trend, where the two waveforms behave in an opposite way.

VI-4 TREE INCEPTION MODEL

The electrical tree inception under AC voltage is commonly related to the number of polarity reversals [98]. The Tanaka and Greenwood model [59] (see equation III-3) theorizes the dependence of the tree initiation with the energy accumulated in the material, which is proportional to the frequency. Therefore, in solid dielectrics an increase of the applied voltage frequency leads to a decrease of the inception voltage or of the time to inception. This energy accumulation is,

however, possible only in solids: liquid and gaseous dielectrics have a completely different behavior in presence of charge injection. Their physical state implicates a difference mechanism of charge transportation and accumulation.

As already deeply discussed in this work, the silicone gel has a behavior intermediate between liquids and solids [75]. The experimental results carried out on silicone gel and presented in chapter V-1 highlight as an increment of the frequency of the applied voltage does not facilitate systematically the tree initiation. The TIV, indeed, increases with the frequency under square voltage. Even looking to the time to inception (that has been not considered a useful parameter to evaluate the tree in gels), the time required to initiate the tree is longer in the higher frequencies (if the time spent at each voltage step is constant, the higher is the TIV recorded, the longer is the test). Moreover, considering the number of polarity reversal required to initiate the electrical tree, the difference is even wider between lower and higher frequencies. Therefore, the inception mechanism in silicone gel must have some peculiarities compared to the mechanism in solid dielectrics and it should have some relation with its partially liquid nature.

Due to the last considerations, the inception model formulated in this work do not take into account an accumulation of damage during the tree initiation in silicone gel. Following this concept, the equation III-3 by Tanaka and Greenwood change into a simple threshold equation:

$$(G_n - G_{th}) \geq 0 \quad (7)$$

thus it is required a single event G_n capable of exceeding the resistance of the material, which is represented by the threshold value G_{th} . Therefore, the definition of the inception mechanism corresponds to the identification of the parameter influencing G_n and G_{th} .

In silicone gel, the first detectable appearance of the inception is a bubble with dimensions in the order of few microns, as shown in Figure VI-6.

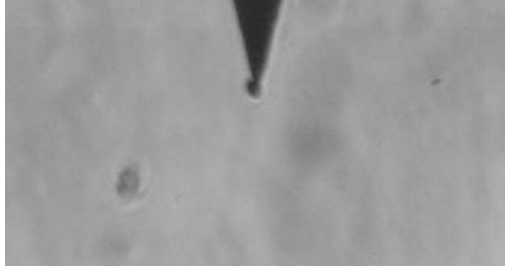


Figure VI-6: Initial bubble shape of electrical tree in gel

The presence of gas dissolved in a liquid is common and, despite an accurate degassing process, unavoidable. Moreover, a small amount of dissolved gas may be produced during the gel cross-linking or through the vaporization of a small amount of the liquid component fraction of the gel by joule heating from the injection/extraction currents.

The physics of a bubble inside a fluid and its equilibrium are described by the Rayleigh-Plesset equation [99], [100], which is an ordinary differential equation explaining the dynamics of a spherical bubble in a liquid, considering this last as an infinite medium.

$$\frac{P_B(t) - P_l(t)}{\rho_l} = R \frac{d^2R}{dt^2} + \frac{3}{2} \left(\frac{dR}{dt} \right)^2 + \frac{4\nu_l}{R} \frac{dR}{dt} + \frac{2S}{\rho_l R} \quad (8)$$

In Equation V-8, R is the radius of the bubble, P_B and P_l are the pressures respectively within the bubble and in the external fluid, ρ_l and ν_l are the density and the kinematic viscosity of the surrounding fluid and its and S is the surface tension. In a static case, the last equation can be rewritten as follow:

$$\Delta P = \frac{2S}{R} \quad (9)$$

which is a simplified form of the Young-Laplace equation. It is clear that bubble formation, growth, and equilibrium are driven by pressure variations.

During inception, the electrical stress and, therefore, injection and extraction must produce the pressure difference required for the formation of the bubble.

Considering again the calculation presented in chapter VI-3, the space charge ρ produced by charge injection is assumed to be spatially uniform over the space charge volume, v , hence, ρv is the total charge accumulated close to the high voltage electrode. The space charge inside the material limits the actual electric field in the region. From a mechanical point of view, considering the external surface of the space charge layer as S_{sc} , it is possible to define a parameter u that can be regarded as the pressure produced by the region of charged silicone gel upon the surrounding material when acted on by the electrode field E :

$$u = E\rho v/S_{sc} \quad (10)$$

This pressure can be seen as the force per unit of surface carried out by the layer of material with space charge on the remaining surrounding part of the dielectric. The u parameter, here defined as *field pressure*, is particularly relevant during the polarity inversion, when the space charge, ρ , and the electric field, E , have opposite sign. In this case, indeed, the force produced by the space charge layer tends to detach the layer from the surrounding medium, creating a void. In other words, during polarity reversal, u represents a depression generated by the interaction between space charge and electric field. This rapid pressure change occurring in a small area can bring to cavitation phenomena, which may be the cause of the electrical tree inception.

The assumption of a limited zone of space charge accumulation, used for the calculation shown in the previous paragraph, may produce unrealistic results in the determination of the field pressure. The space charge distribution, indeed, is likely inhomogeneous and transport and diffusion phenomena should occur outside the space charge layer impeding the formation of a neat discontinuity. Therefore, the actual values of u obtained from the model previously employed may not correspond to a real physical value. Nevertheless, their trend is realistic, since the inhomogeneous distribution inside the layer and the diffusion outside it effect similarly under every voltage waveform. In a real case, in fact, the pressure difference required to trigger the supposed cavitation is due to a significant

difference between the space charge in two consecutive layers of silicone gel. Likely, in a pin-plane electrode configuration, it occurs along the pin axis direction and extremely close to the pin electrode within the gel matrix.

The electrical tree inception mechanism in silicone gel should be connected to a pressure variation. In order to continue with the term used until now, the values of G_n and G_{th} have to be related to the pressure of the dissolved gasses and to the pressure of the silicone gel. In this dissertation, the G_n is related to the presence of gasses inside the gel and thus is the parameter not influenced by the electrical field; furthermore, it can include the other terms, such as the surface tension and it should be influenced by external pressure, temperature and moisture. G_{th} , instead, depends by the pressure inside the silicone gel and thus it is influenced by the space charge pressure wave.

$$G_{th} \propto uF \quad (11)$$

The field pressure depends on temperature, T , by the physical properties of the material since is connected with the parameters controlling the injection current (here α and β), the applied voltage, V , and its derivative with respect to time. It is reasonable to envision that G_{th} should be dependent to the room pressure of the gel, as well as to the moisture and other parameters that have not been investigated into this work and may require further investigations. The term F in equation VI-11 should include all these dependences.

Hence, the inception model proposed here is based on a single event, where the space charge in the region close to the injecting electrode creates a pressure wave sufficiently intense to exceed a material threshold value.

VI-5 MODEL VALIDATION

In order to compare the experimental results with the model proposed, some simplification should be performed.

The field pressure is dependent by the applied voltage. Both E and, particularly, ρ are, indeed dependent to V . Nevertheless, in first approximation, in a neighborhood of a fixed value of V_{pk} , u can be normalized becoming proportional to the applied voltage peak value V_n :

$$u_n V_n = u \quad (12)$$

and thus, when the voltage used to normalized the field pressure, is equal to the inception voltage:

$$G_{th} \propto u_n V_i F \quad (13)$$

where V_i is the tree inception voltage. With this simplification, it is possible to compare easily the experimental results obtained in the TIV tests and the inception model. Following the model, indeed, G_n is equal to G_{th} in the tree initiation, therefore:

$$V_i \propto \frac{G_n}{u_n F} \quad (14)$$

Equation VI-14 enunciates that the inception voltage is inversely proportional to the field pressure. This is valid considering small variation of the voltage with respect to the one used in the calculation. In the experimental condition employed, F is considered a constant, thus, for the clarity of the subsequent evaluation, it is possible to write the parameter φ :

$$\varphi \propto \frac{1}{u_n F} \quad (15)$$

which is proportional to the TIV.

A first comparison between the experimental value of TIV_n and the calculation is proposed in Figure VI-7. In this case, φ is calculated for 9 kV_{pk} voltage and both the experimental tests and the calculation are performed with a high-voltage electrode radius of 5 μ m. The constant value of F is chosen to adjust

the φ values in order to be comparable with the TIVn, since the aim is to compare the trends of φ and TIVn, but it has been used the same value of F for all the figures which follow.

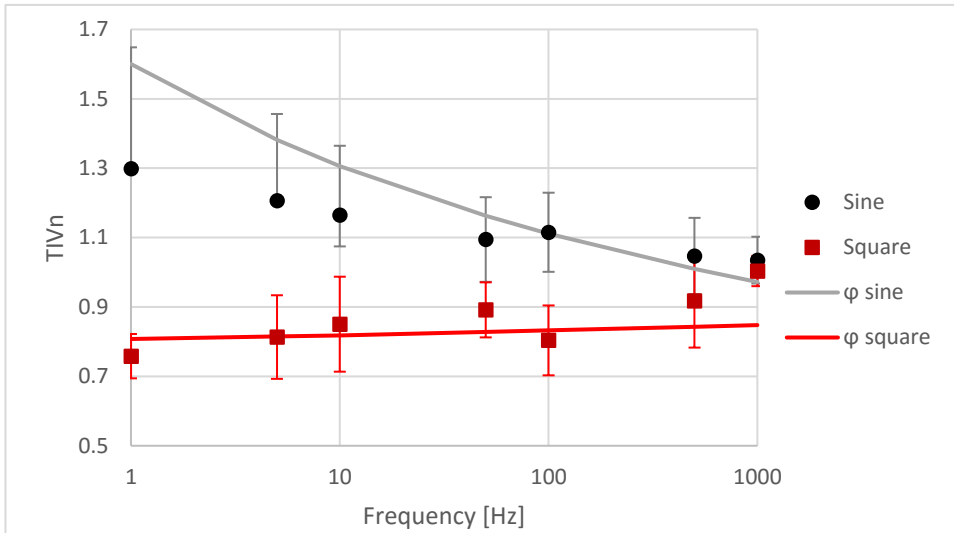


Figure VI-7: TIVn results for 5 μm radius tip and φ trends

The small increase with the frequency of φ calculated for the square voltage waveform is comparable with the one measured in TIVn for the square voltage. Moreover, comparing the sinusoidal and the square voltage results, the ratio between the different TIV seems to be approximately the same as the one between φ calculated for the square and sinusoidal voltage. In order to confirm this trends, Figure VI-8 shows the TIVn recorded with the 3 μm radius tip needle and the values of φ calculated for a voltage applied of 6 kV_{pk} .

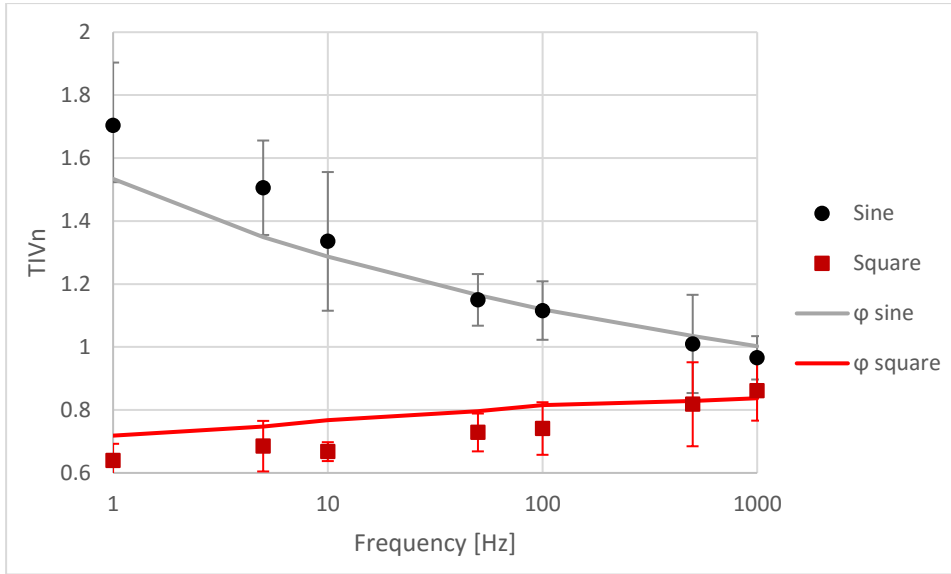


Figure VI-8: TIVn results for 3 μm radius tip and ϕ trends

The correlation between the calculated data and the experimental results is confirmed and even more evident in this second graph. Both the figures highlight a small discrepancy between ϕ and the TIVn at the lower frequency in the sinusoidal voltage. This is due in part to the higher experimental error occurred for these values and in part to the intrinsic limit of the model. Indeed, the calculation is made with a series of approximation, e.g. the last one in the treatise is to consider V_i proportional to u , which can be not completely true for these low rise time waveforms or for this applied fields. Nevertheless, the correspondence between the trends of the calculated field pressure and the TIVn is confirmed also with different rise times. In Figure V-8, for example, the experimental results obtained with the square voltage with 250 V/ μs and 12.5 kV/ μs slew rate are compared, showing an average decrease of about the 13% of the TIVn increasing the slew rate. From the comparison between the ϕ values obtained with the two slew rates at 9 kV_{pk}, it has been recorded a decrease of about the 18% between 250 V/ μs and 12.5 kV/ μs , showing that, also in this comparison, the field pressure is well approximating the trend of the inception voltage. This good agreement was found even though at the high slew rate the effective time where u is at its

maximum value is extremely short and it may be possible for the direct proportionality between TIV and φ to be lost. For shorter rise time, the model may become weak, since the waveform tends to an impulsive shape and the inception mechanism may be different. In any case, the model seems to be reliable down to values of rise time considerably short for technical applications.

The mathematical model used for the calculation of the space charge and the electric field in the region close to the high voltage electrode is not appropriate to be used with unipolar waveforms. The behavior of the space charge during the rise and fall time, since the actual voltage is never reversed, can be difficult to be predicted. The SCLF is easily reached for the range of voltage employed in the experiments carried out in this work and the measurement results presented in chapter V-1.3 highlight a strong similitude with the results obtained with the bipolar square voltage at the same applied peak voltage. Thus, even though further analysis and a proper injection model should be done for the unipolar case, from a practical point of view, the estimation of the tree inception voltage in silicone gel under unipolar square waveform can be performed using the same model used for the bipolar waveforms, possibly adopting a safety coefficient (close to the unity, e.g. 0.9) for the application tests.

VII ELECTRICAL TREE GROWTH

The electrical tree inception in silicone gel has an unconventional and unexpected origin if compared with solid dielectrics. Therefore, it is presumable, that the growth process in the gel and solids are different. Indeed, the well-known self-healing capability of silicone gel should be active in this phase of the electrical treeing. Moreover, the propagation of the tree occurs following in part a bubble-mechanism, unique in the dielectrics, as explained in this chapter.

VII-1 TIME AND LENGTH OF TREES

For solid dielectrics, the geometric parameters employed to analyze the electrical trees are the length (alternatively, the minimum distance from the ground electrode), and the fractal number. The time to cross the insulation and the time to breakdown are also reported usually, noting that breakdown does not ensue immediately at the time the tree bridges the electrodes: the tree channels should be enlarged to a minimum diameter, which depends by the dielectric, often at least 5 μm , to allow a full discharge of the insulation [37].

Some peculiarities of silicone gel have emerged from experimental results. First, due to the self-healing property of the silicone gel and its semi-liquid nature, the tree shape is not stable. Therefore, an accurate calculation of the fractal number is often very difficult and inaccurate. Owing to the above limitations, the fractal number is not calculated here, but it is exclusively assessed to compare the effects associated with different voltage waveforms. Second, the time to cross the insulation and the time to breakdown coincide in silicone gel: the tree, in fact,

instantly short-circuits the insulation when it reaches the ground electrode. Finally, due to the self-healing property, the maximum length reached by the tree often does not correspond with the last position reached by the tree, as it is common in solid dielectrics.

Deterministic chaos was advocated in [101] to explain tree growth. Consequently, the tree shape was modeled assuming it was a statistical fractal. To characterize fully phenomena driven by deterministic chaos, an enormous number of tests would be necessary and, even in that case, the prediction of the time to breakdown would be largely erratic. Therefore, the experimental analyses reported from now are aimed exclusively at describing the tree growth and its underlying mechanisms.

VII-1.1 Time to breakdown (TTB)

The tree growth tests were performed following the procedure explained in chapter IV-2.2, at a fixed voltage of 10 kV_{pk}. The TTB reported here coincides with the time to cross the insulation for both the silicone gel and the elastomer. This choice is not common for the latter, as the TTB in solids is actually larger than the time to cross the insulation.

The most striking observation comes from evaluating of the trend of the TTB with the frequency. Table 2 shows the TTB of silicone gel sample under sinusoidal and square voltage (250 V/μs), while the results obtained for the elastomer are shown in Table 3. Each cell in the tables corresponds to a different sample tested.

1 Hz SINE	1 Hz SQUARE	50 Hz SINE	50 Hz SQUARE	1 kHz SINE	1 kHz SQUARE
-	-	-	14.25	0.83	0.58
-	-	-	-	3.5	0.72
-	-	-	-	60.5	3.25

Table 2: Time to breakdown in silicone gel samples [min]

50 Hz SINE	50 Hz SQUARE	1 kHz SINE	1kHz SQUARE
-	8	4.59	1.88
-	-	5.75	5.25

Table 3: Time to breakdown in elastomer [min]

Even if the sample size is very limited, due to the large variance of TTB values some comparisons are possible. At 1 kHz, TTB is shorter for the gel samples compared with the elastomer ones. The inverse occurs for 50 Hz. This dependence on frequency is ascribable to the gel self-healing property: the time constant for self-healing is probably too high to prevent the tree growth at 1 kHz. On the contrary, self-healing phenomena become important at 50 Hz and suppress tree growth at 1 Hz. Using sinusoidal voltages, the gel strain due to the space charge injection is too low to sustain the tree, which collapses few seconds after the inception (the tree was incepted using square voltages owing to their lower TIV). Under square voltages at 1 Hz, the tree can grow significantly, but the gel is capable of contrasting its growth, leading to a continuous process of expansion and contraction of the tree. Indeed, the tree did not reach the ground electrode during the two hours tests.

For solid dielectrics (silicone elastomer can be regarded as a solid dielectric), the time to breakdown is approximatively proportional to the frequency of the applied voltage [37]. For silicone gel, the increase of frequency can lead to a sudden growth of the tree when the amount of damage per unit time exceeds the self-healing capability. Thus, the dependence on frequency is super-linear and warns extreme caution.

Considering that power modules are subjected to unipolar voltages, tests have also been carried out on silicone gel samples under unipolar square voltages at 20 kV_{pk-pk}. The results are reported in Table 4.

1 Hz POSITIVE	1 Hz NEGATIVE	50 Hz POSITIVE	50 Hz NEGATIVE	1 kHz POSITIVE	1 kHz NEGATIVE
10.1	85	8.1	5.75	0.5	1.1
98	-	-	64	1.88	2.92

Table 4: Time to breakdown in silicone gel samples under unipolar waveforms [min]

The data lead to the conclusion that, regarding the velocity of growth, unipolar voltages are more dangerous compared to the bipolar one. Indeed, one should bear in mind that the peak voltage of unipolar voltage is twice that of bipolar voltages (the peak-peak voltage is the same). Since the growth mechanism is driven by the propagation of discharges inside bubbles or hollow channels, the higher voltage reached in the unipolar voltage can incept PD of larger magnitudes (that will create more damage and larger bubbles since they will release larger amounts of gasses) and may inject larger space charge in the gel. This space charge would help to (a) elongate the bubbles in the direction of the field, and (b) create secondary bubbles through the space charge differential strain. This justifies the higher growth velocity.

Finally, some tests have been performed on silicone gel with 10 kV_{pk} bipolar square voltages with a 12.5 kV/ μ s slew rate. The results are shown in Table 5. The

increase in the slew rate reduces slightly the TTB. Therefore, the gas ionization process inside the bubbles and the channels should be stronger compared with the 250 V/ μ s tests. Contrary to what happens with the unipolar waveforms, the tree growth is not accelerated appreciably at 1 Hz. The difference between the two slew rates could be associated with stronger PD associated with larger slew rates. This phenomenon has been observed in twisted pairs [102] and explained through the effect of stochastic delay in PD inception.

1 Hz HSR-SWG	50 Hz HSR-SWG	1kHz HSR-SWG
-	8.9	1.1
-	13	4.5

Table 5: Time to breakdown (in [min]) of gel samples under square voltages having slew rate of 12.5 kV/ μ s

VII-1.2 Maximum length and fractal number

The analysis of the tree shape is a common *a posteriori* evaluation on the damage caused by the electrical treeing. For the silicone gel, due to self-healing property of the gel, the tree morphology undergoes continue fluctuations. Therefore, the analysis should be carried out during the tree development, using pictures obtained at regular times.

In the tests where the tree did not reach the ground electrode, the minimum distance between the tip of the tree and the ground electrode has been detected and reported. In Table 6 are shown the results for the silicone gel samples, while the minimum distance reached by the elastomer are reported in Table 7.

1 Hz SINE	1 Hz SQUARE	50 Hz SINE	50 Hz SQUARE	1 kHz SINE	1 kHz SQUARE
2.8	0.6	2.3	0	0	0
2.8	1	2.4	0.45	0	0
2.9	2.4	2.6	0.6	0	0

Table 6: Minimum distance (in [mm]) of the tree from the ground electrode in silicone gel

The evaluation of the minimum distance from the ground electrode reached by the tree in silicone gel highlights a significant difference between sinusoidal and square voltages. At 50 Hz, the square voltage always arrived close to the ground and, thus, to the breakdown. On the contrary, the sinusoidal waveform created just a small branch tree localized close to the needle tip. At 1 Hz, the difference is even more evident: under sinusoidal voltages, the tree collapses after few seconds, leaving the sample with no significant damage. The square voltage creates a tree with, often, a single branch but often able to achieve a considerable length.

For the elastomer, the tree length shows a similar dependence on sinusoidal and square voltages. As before, tree growth is explained by the PD development. PDs occur inside the gaseous channels forming the tree when it is initiated. The intensity of PD is linked to the derivate of the voltage applied, with stronger discharges when the \dot{V} is higher, at least within a certain range of \dot{V} values. Therefore, since tree growth is due to PD activity, it is possible to conclude that the square voltage should have a higher growth ratio than sinusoidal one. Moreover, because in sinusoidal waveform the \dot{V} depends on the frequency, the difference between square and sine voltage should be wider at the lower frequencies and smaller at the higher. This speculation is confirmed by the data.

50 Hz SINE	50 Hz SQUARE	1 kHz SINE	1kHz SQUARE
2.1	0	0	0
2.3	1.4	0	0

Table 7: Minimum distance of the tree from the ground electrode in elastomer [mm]

The tree shape of a vented tree is defined by his fractal number and classified according to the terminology explained in chapter III-2.1.

In this work, the shape of the trees was observed optically during their growth and some important consideration can be outlined. First, the tree inside silicone gel is formed through a series of bubbles produced at the tree branch ends, which leave some channels. Both the channels or the bubbles may reclose due to the self-healing properties of the material. This propagation through bubbles is a peculiarity of the electrical tree inside the gel and will be discussed deeply in the next paragraph.

A second important outcome of the shape evaluation process regards the fractal number, which is dependent on the frequency. At 1 kHz, the number of branches produced in the silicone gel is high. Thus, the tree can be classified as a branched tree with a significant fractal number. The relevant amount of bubbles produced simultaneously covers almost completely the tree on the 2D optical plane. The fractal number decreases with the frequency, but at 50 Hz, the tree is still branched. The aspect changes when the voltage is further decreased. At 1 Hz, the tree is almost represented by a single main tree with very few branches. Thus the fractal number is low. A similar trend is observable in the elastomer. The fractal number at 1 kHz is slightly higher than the one at 50 Hz. However, in both the cases, the tree appears with more branches than in the silicone gel. The tree obtained in the tests on elastomer at 1 kHz is close to a bush tree.

Figure VII-1 shows some examples of trees. The images confirm the discussion carried out just above on the fractal number in the different cases. It is

noteworthy the presence of bubbles in the first tree images, referring to the silicone gel samples. In the case at 1 kHz (lower left), a number of bubbles is extremely high, highlighting a fast growth phase.

The tree in the elastomer, since it is a solid dielectric, does not show any bubble. Moreover, the channels appear thinner compared to the ones developed in silicone gel.

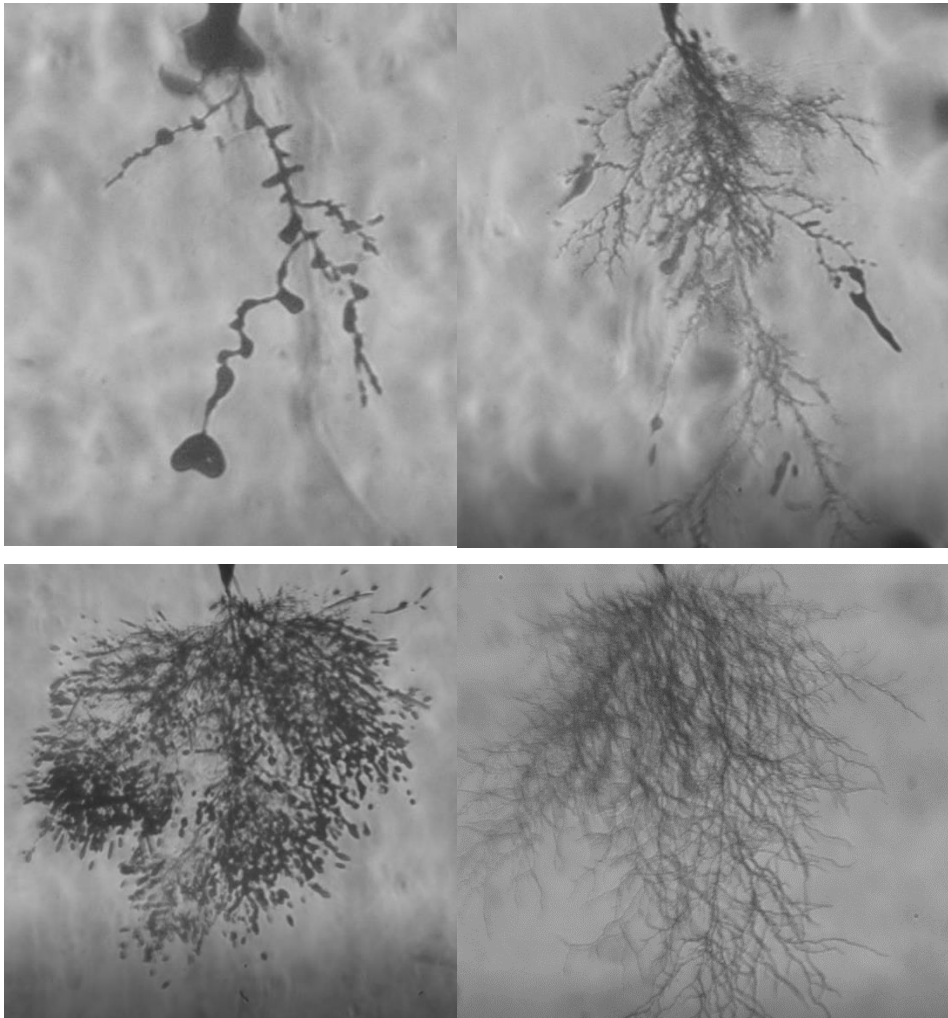


Figure VII-1: Tree shape in gel at 1 Hz square (upper left), 50 Hz square (upper right), 1 kHz sine (lower left) and in elastomer at 1 kHz sine (lower right)

VII-2 GROWTH MECHANISM IN GEL

The inception of the electrical tree in silicone gel has been described in this work through a mechanism that has been postulated also for solid dielectrics, but less likely to occur on a short time scale due to the high yield strength of solids [103]. The fluid-like features observed in the gel are the main reasons for this choice. The clearest evidence of the semi-fluid nature of silicone gel is the presence and the development of gas bubbles inside it. These bubbles, besides being the first sign of the tree inception, are leading the tree growth mechanism too. In silicone gel, indeed, the tree may appear as a filamentary branched backbone such as occurs in solids but around its periphery there are bubble-shaped cavities that may collapse and separate from the backbone just as in liquid streamers, leaving free bubbles inside the gel.

Some investigations were carried out on the bubble motion by other authors [104] in recent years. They tried to connect the bubble motion with the sinusoidal voltage applied. In this thesis work, the investigation of the bubble motion and generation was easier because of the possibility to use a wide range of frequencies and two different waveforms.

Through the tree inception, a small bubble is placed in contact with the high voltage electrode. At this point, the gas inside the bubble is directly in contact with the electrode and the PD may easily start. In this configuration, the PD development is not far from the one occurring in common electrical treeing inside solid dielectrics. The discharges are, influenced by the electrical field variation due to the high voltage source waveform. The molecules of ionized gas in the bubbles are directed by the electric field and push on the bubble surface leading to the growth and the movement of the bubbles in a direction almost parallel to the field. Moreover, the PDs may create an accumulation of space charge on the bubble surface, that concurs on influencing the bubble movement. The path of the

gas followed during this motion from the high voltage to the ground forms the tree channels.

The channel formed by the gas movement can develop in three manners, depending on the gas movement and the self-healing property of the gel. It can:

- collapse immediately after the bubble passage, thus closing its connection with the high voltage electrode;
- maintain its shape for a certain period until the ionized gas flows repeatedly inside it and move the bubbles further, collapsing as soon as this flow is missing;
- create a stable channel, similar to the one which may occur in solid dielectrics.

The first development is similar to what usually occurs in liquids, furthermore, it has been revealed common when the silicone gel is formed with an inappropriate ratio between the two base compounds, leading to a more liquid mixture [77]. In this last case, the bubbles produced during the inception can be considered streamers. When the correct A:B ratio is employed in the manufacturing process, the immediate collapsing of the channels may occur both at the lower frequencies, when the plasma gas flow is not enough to sustain the channel, or when the bubbles are pushed too far from the generation point, even in the presence of significant electric stress. This rapid collapse of the channel brings the gel to behave as a liquid and this can be considered the first very fast self-healing. When this development occurs, some bubbles of charged gas are formed and released inside the gel.

The channels can also collapse after several seconds, sometimes minutes, after their creation. This second case is the most interesting self-healing phenomenon in the silicone gel since it cannot be associated with a pseudo-liquid behavior. The channels, in this case, appear well-formed, and the bubbles and the tree are advancing inside the material. Nevertheless, due to the erratic trend of PDs and consequently of gas ions, the flow in a channel can drop and cease, even

for a short time. In this case, the mechanical properties of the gel lead the material to return to its original shape, thus decreasing the channel diameter, while the liquid phase inside the gel may fill the rapidly the fracture left by the channel. This is what is defined as stage 1 of the self-healing process by Salvatierra et al [77].

Finally, when the self-healing is not occurring in the channel, this become a stable branch of the tree. A second self-healing process may occur, accordingly to [77], called Stage 2, which requires some hours and is possible only if the electric stress on the silicone gel is completely shut down. This long process should be carried out by the liquid phase of the gel, which completely fills mechanically stable channels. This work did not evaluate this particular self-healing mechanism, since it is relatively useless for real applications, which may run continuously.

The observation of the tree growth mechanism has been possible only evaluating the several videos recorded during the tree development inside the samples. The measurements carried out at 1 Hz singled out some important features that, with higher frequencies, would have required special acquisition systems, such as a high-speed camera. An important evidence regards the charge of the ions forming the gas bubbles, which can be indirectly evaluated thanks to the bubble motion. In the videos, indeed, the bubbles are moving at the same frequency of the electrical field, and bubble formation takes place at the needle tip during polarity inversions, when stronger PDs take place. Firstly, it is clearly detectable that the bubbles are formed at a frequency approximately twice that of the applied voltage, thus both during positive than negative phase. Secondly, in the growth process, some bubbles are attracted to the high voltage electrode, while other ones are rejected. This is simply due to the charge of the gas ions trapped inside the bubble since the charge does not change after the separation from the electrode. Similar conclusion regarding the charge trapped in the bubbles were obtained by [104], therefore confirming that both positive and negative charge

carried are involved in the tree growth. Figure VII-2 refers to two frames captured on the same sample tested at 1 Hz.

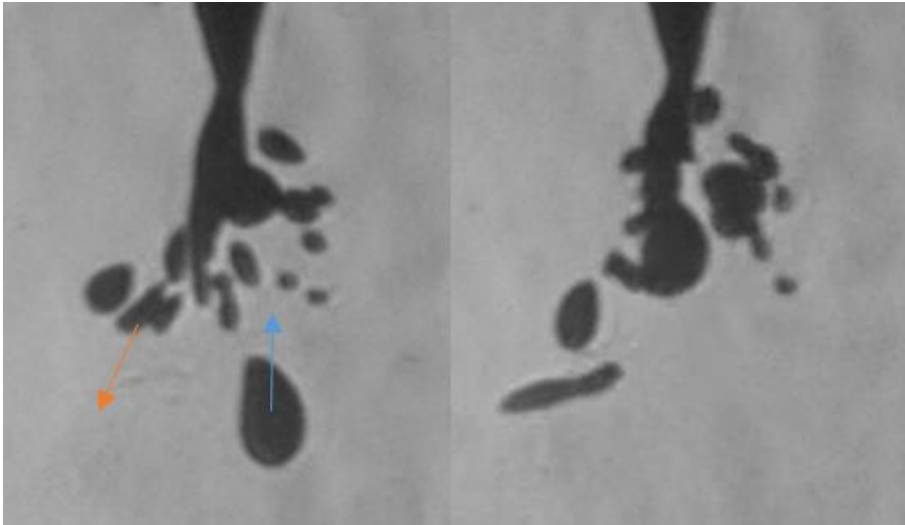
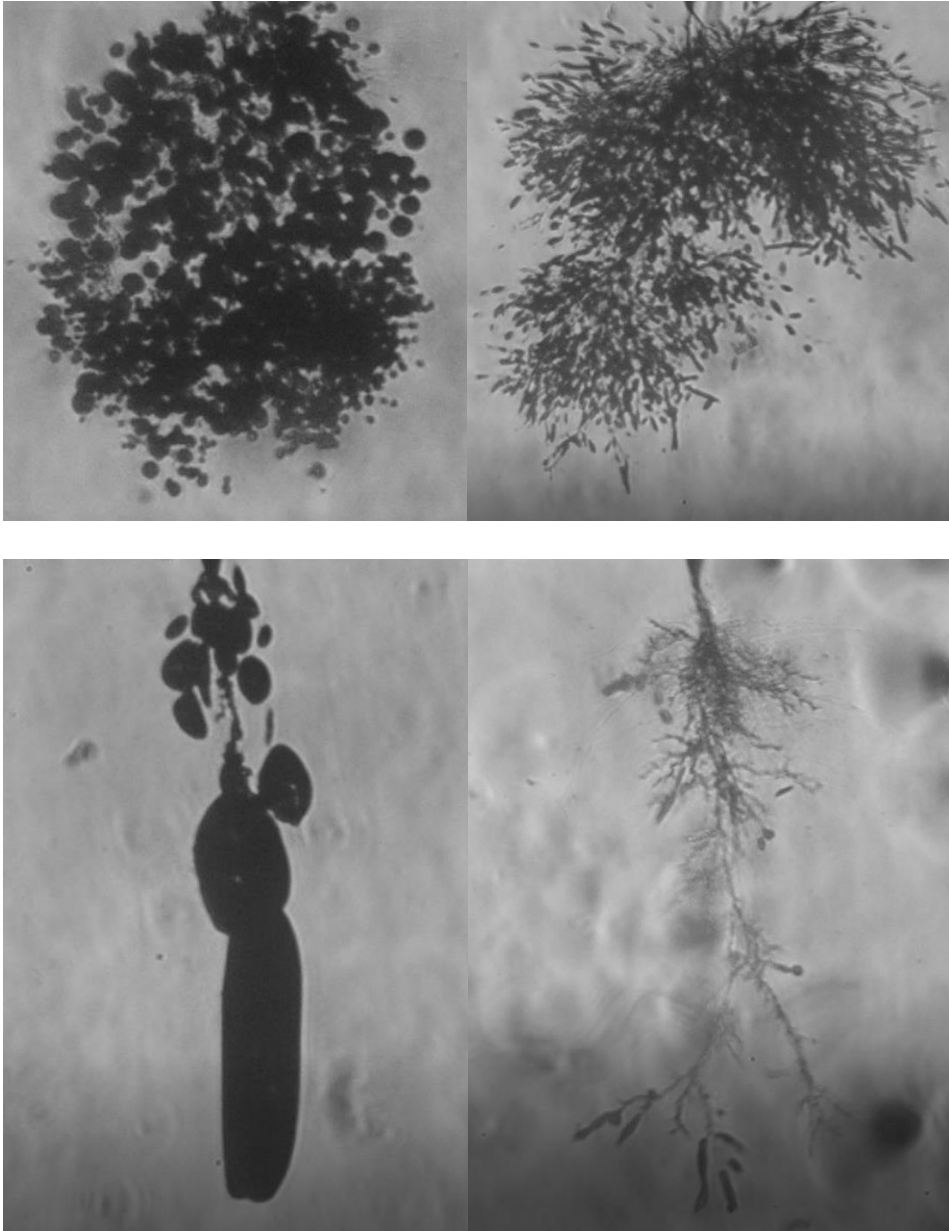


Figure VII-2: Bubbles opposite movement under electric field due to their internal charge

The two frames are taken at 0.5 seconds, showing the movement of the bubbles under the electric field. While some bubbles get closer to the electrode, others are leaving it.

The bubbles observed during the tree growth tests showed a wide range of shapes. In general, the largest bubbles were reported at 1 Hz, where they are filled with a major quantity of gas produced by PDs while the voltage is at its maximum values.. Moreover, the bubble obtained and continuously filled during several PD events may have not symmetrical shape.

At higher frequency, the bubbles tend to be more symmetric usually with an ellipsoidal shape or sometimes even spherical. Some examples are shown in Figure VII-3.



*Figure VII-3: Bubble development examples.
Upper left: numerous spherical bubbles obtained at 1 kHz sine.
Upper right: numerous oblong bubbles obtained at 1 kHz square.
Lower left: huge bubbles with random shapes obtained at 1 Hz square.
Lower right: few oblong bubbles obtained at 50 Hz square*

The four main cases are presented in the images:

- the tree can grow creating a significant amount of (almost) spherical bubbles, which partially cover the tree itself from the optical detection;
- the PD can create a considerable number of oblong bubbles, and this is the worst case, usually reaching the maximum tree growth rate;
- few big asymmetrical bubbles, common at very low frequencies as explained before;
- few oblong bubbles, which lead the tree growth developing from its extremities.

It has not been possible to relate clearly the shape or the creation rate of the bubbles to the waveform and the frequency. In general, the trees with the higher number of bubbles are the ones obtained at the higher frequencies. Sinusoidal and square voltages can generate either oblong or spherical bubble.

Considering the charge injected, it appears that the polarity of the ionized gas filling the bubbles does not influence the bubble shape. Moreover, during the tree growth at the higher frequencies, the difference between the two possible ion signs are less evident and influential in the tree development: the time constant of the bubbles are too long. Thus the bubbles do not oscillate following the electric field. Instead, they can only collapse thanks to the self-healing or be the starting point of the successive tree branches.

VIII CONCLUSIONS

This work examined the key aspects of the electrical treeing inside silicone gel. As expected, the gel-like nature of the material required to evaluate the phenomenon from a new point of view compared to the classical studies on electrical treeing, which were performed only on solid dielectrics.

The first and most important result of this work is a reliable model to predict the tree inception under different voltage waveforms. The model relates the inception to a cavitation process. This cavitation is caused by a depression inside the silicone gel, in the zone of the material in contact with the high voltage electrode. The depression ensues the voltage polarity reversal, when layers of silicone gel, charged with opposite polarity with respect to the electric field, are attracted to the high voltage electrode with different forces.

Due to the approximations employed, the results of the model should be considered exclusively to compare different waveforms. Indeed, the model has been envisaged to assess the dangerousness of different waveform and frequency and for this purpose is entirely useful. The experimental data confirmed its validity. The prediction of the inception voltage under determined geometrical and electrical boundary conditions is extremely relevant: after the inception, despite the self-healing process, the tree growth and the resulting breakdown are very likely.

Although the model permits reliable prediction, sufficient for practical applications, further implementations are necessary: the space charge should not be considered homogeneous in the material, taking into account transport and

diffusion, thus creating a space charge gradient. Moreover, this kind of model would calculate directly also the field in unipolar waveforms. All these considerations may require a FEM model and they would increase the complexity of the calculation drastically. A less complex improvement may take into account a deeper investigation of other parameters influencing the model proposed in this thesis. The most interesting one may be the correlation of the F parameter of Equation VI-11 and thus a study regarding the pressure of silicone gel (or the mechanical stress, depending if the gel is considered liquid or solid), therefore a further research may carry out experimental tests with this purpose.

Following the model, the main risk factor can be considered the length of rise and fall times of the voltage waveform: the shorter the rise time, the higher the failure probability. A low frequency square voltage results to be the riskiest condition for an electrical insulating system made by silicone gel, at least for the electrical tree inception, following the calculations made. Nevertheless, square voltage waveforms in general and high-frequency sinusoidal waveform should be considered as a high risk too. Finally, considering the results of this work as preliminary guidelines for establishing reliability tests, it may be wise to introduce a safety factor which, taking into account the non-uniformity of the silicone gel and the randomness of the phenomenon, would decrease the calculated inception voltage.

The prediction of electrical tree growth is extremely complex in solid dielectrics. In silicone gel, the complexity is even greater as behaviors typical of liquid and solid materials are both observable. The PD occurring in the gas filled bubble-shaped channels are the engine of the tree. The bubbles are an element feasible only in a liquid and their movements have been characterized in this work. Particularly, it has been noted that they can be produced and filled both by positive or negative ions and their shapes has been related to the voltage waveform, at least in part.

The tree develops through the continuous creation and movement of the bubble-shaped cavities, which may leave behind, depending on the self-curing capability of the silicone gel, a backbone of stable channels thinner than the bubbles but almost irreversible. This behavior has analogies with electrical treeing in solids.

The experimental evidence highlighted the dangerous of the higher frequencies, where the self-healing process is not able to reduce the damage produced by the PD in the gas channels. Moreover, it appears that the unipolar waveforms are worse than bipolar ones at the same level of voltage peak-to-peak. The aim of the analyses on electrical tree growth on silicone gel is to the instruments to understand the physics behind this elaborate phenomenon, in order to achieve a sufficient level of knowledge of the mechanism occurring in this material in between solid and liquid dielectrics.

REFERENCES

- [1] W. Noll, *Chemistry and Technology of Silicones*. Academic Press, 1968.
- [2] H. H. Moretto, M. Schulze, and G. Wagner, “Silicones,” in *Ullmann’s Encyclopedia of Industrial Chemistry*, 2007, pp. 1–40.
- [3] D. D. Dickson, “An overview of silicone dielectric gels,” in *Electrical/Electronics Insulation Conference, EIC*, 1975, no. Table 3, pp. 92–95.
- [4] T. Ebke, A. Khaddour, and D. Peier, “DEGRADATION OF SILICONE GEL BY PARTIAL DISCHARGES DUE TO DIFFERENT DEFECTS,” in *Dielectric Materials, Measurements and Applications, 2000. Eighth International Conference on*, 2000, pp. 202–207.
- [5] J. Banaszczyk and B. Adamczyk, “Dielectric strength measurements of silicone gel,” in *Progress in Applied Electrical Engineering (PAEE)*, 2016.
- [6] Y. Liu, *Power Electronic Packaging*. Springer, 2012.
- [7] C. Durand, M. Klingler, D. Coutellier, and H. Naceur, “Power Cycling Reliability of Power Module: A Survey,” *IEEE Trans. DEVICE AND MATERIALS Reliab.*, vol. 16, no. 1, pp. 80–97, 2016.
- [8] T. A. T. Vu, J. Augé, O. Lesaint, and A. Test, “Low Temperature Partial Discharge Properties Of Silicone Gels Used To Encapsulate Power Semiconductors,” in *Annual Report - Conference on Electrical Insulation and Dielectric Phenomena, CEIDP*, 2009, pp. 421–424.

- [9] C. P. Wong, "Thermal-Mechanical Enhanced High- Performance Silicone Gels and Elastomeric Encapsulants in Microelectronic Packaging," *IEEE Trans. Compon. Packaging. Manuf. Technol.*, vol. 18, no. 2, pp. 270–273, 1995.
- [10] M. Ciappa, "Selected failure mechanisms of modern power modules," vol. 42, pp. 653–667, 2002.
- [11] M. Berth, "Partial Discharge Behaviour of Power Electronic Packaging Insulation," *Int. Symp. Electr. Insul. Mater.*, pp. 565–568, 1998.
- [12] T. Maeda, K. Haga, and T. Maeda, "Creepage Breakdown Characteristics of Printed Wiring Board in Silicone Gel," in *Proceedings of Conference on Electrical Insulation and Dielectric Phenomena - CEIDP*, 1996, pp. 734–737.
- [13] J. Fabian, S. Hartmann, and A. Hamidi, "Analysis of Insulation Failure Modes in High Power IGBT Modules," pp. 799–805, 2005.
- [14] G. Mitic and G. Lefranc, "Localization of Electrical-Insulation- and Partial-Discharge Failures of IGBT Modules," *IEEE Trans. Ind. Appl.*, vol. 38, no. 1, pp. 175–180, 2002.
- [15] D. Frey, J. L. Schanen, J. L. Augé, and O. Lesaint, "Electric field investigation in high voltage power modules using finite element simulations and partial discharge measurements," pp. 1000–1005, 2003.
- [16] H. HOURDEQUIN, L. LAUDEBAT, M.-L. LOCATELLI, and P. Bidan, "Design of Packaging Structures for High Voltage Power Electronics Devices: Electric Field Stress on Insulation," in *IEEE International Conference on Dielectrics*, 2016.
- [17] G. Lefranc, T. Licht, H. J. Schultz, R. Beinet, and G. Mitic, "Reliability testing of high-power multi-chip IGBT modules," vol. 40, pp. 1659–1663, 2000.

- [18] J. L. Augé, O. Lesaint, and A. T. V. U. Thi, "Partial Discharges in Ceramic Substrates Embedded in Liquids and Gels," *IEEE Trans. Dielectr. Electr. Insul.*, vol. 20, no. 1, pp. 262–274, 2013.
- [19] C. Duchesne, E. Dutarde, and P. Electronics, "PB25 Stress grading in integrated power modules," no. Li, pp. 347–351, 2008.
- [20] M. Locatelli, R. Khazaka, S. Diahm, C. Pham, M. Bechara, S. Dinculescu, and P. Bidan, "Evaluation of Encapsulation Materials for High-Temperature Power Device Packaging," *IEEE Trans. power Electron.*, vol. 29, no. 5, pp. 2281–2288, 2014.
- [21] C. Neeb, L. Boettcher, M. Conrad, and R. I. K. W. D. E. Doncker, "Innovative and Reliable Power Modules," *IEEE Ind. Electron. Mag.*, no. September, pp. 6–16, 2014.
- [22] T. Seldrum, E. Vanlathem, V. Delsuc, and H. Enami, "New silicone gel enabling high temperature stability for next generation of power modules," in *International Exhibition and Conference for Power Electronics, Intelligent Motion, Renewable Energy and Energy Management*, 2016, pp. 1017–1020.
- [23] H. G. Yaworski, G. Craig, and D. Roberts, "The Use of Silicone Gels for Jointing Power Cables," in *Transmission and Distribution Conference*, 1996, pp. 396–401.
- [24] H. G. Yaworski and R. Bukovnik, "Silicone Gel Technology For Power Cable Accessories," in *Transmission and Distribution Conference and Exposition, 2001 IEEE/PES*, 2001, pp. 837–842.
- [25] R. R. Bukovnik and P. R. Carey, "Advances in Silicone Gel Technology for Cable Accessories," in *IEEE/PES Transmission and Distribution Conference and Exhibition*, 2006, pp. 1–4.
- [26] "IEC 60270:2000, High-voltage test techniques - Partial discharge

measurements.” 2000.

- [27] W. Hauschild and E. Lemke, *High-Voltage Test and Measuring Techniques*. 2014.
- [28] J. C. Devins, “THE PHYSICS OF PARTIAL DISCHARGES IN SOLID DIELECTRICS,” *IEEE Trans. Electr. Insul.*, vol. EI-19, no. 5, pp. 475–495, 1984.
- [29] A. Pedersen, “On the Electrical Breakdown of Gaseous Dielectrics An Engineering Approach,” *IEEE Trans. Electr. Insul.*, vol. 24, no. 5, pp. 721–738, 1989.
- [30] P. H. F. Morshuis, “Partial Discharge Mechanisms. Mechanism Leading to Breakdown, Analyzed by Fast Electrical and Optical Measurements,” Delft, 1993.
- [31] A. Cavallini, G. C. Montanari, F. Puletti, and A. Contin, “A New Methodology for the Identification of PD in Electrical Apparatus: Properties and Applications,” *IEEE Trans. Dielectr. Electr. Insul.*, vol. 12, no. 2, pp. 203–215, 2005.
- [32] A. Contin, A. Cavallini, G. C. Montanari, G. Pasini, and F. Puletti, “Digital Detection and Fuzzy Classification of Partial Discharge Signals,” *IEEE Trans. Electr. Insul.*, vol. 9, no. 3, pp. 335–348, 2002.
- [33] E. H. Rayner, “HIGH-VOLTAGE TESTS AND ENERGY LOSSES IN INSULATING MATERIALS,” *J. Inst. Electr. Eng.*, vol. 49, no. 214, pp. 3–71, 1912.
- [34] D. M. Robinson, “THE BREAKDOWN MECHANISM OF IMPREGNATED PAPER CABLES,” *J. Inst. Electr. Eng.*, vol. 77, no. 463, pp. 90–103, 1935.
- [35] J. H. Lawson and W. J. Vahlstorm, “INVESTIGATION OF INSULATION DETERIORATION IN 15 KV AND 22 KV

- POLYETHYLENE CABLES REMOVED FROM SERVICE - PART II,” *IEEE Trans. Power Appar. Syst.*, vol. PAS-92, no. 2, pp. 824–835, 1972.
- [36] G. Bahder, C. Katz, J. H. Lawson, and W. Vahlstrom, “ELECTRICAL AND ELECTRO-CHEMICAL TREEING EFFECT IN POLYETHYLENE AND CROSSLINKED POLYETHYLENE CABLES,” *IEEE Trans. Power Appar. Syst.*, vol. PAS-93, no. 3, pp. 977–989, 1973.
- [37] L. A. Dissado and C. Fothergill, *Electrical Degradation and Breakdown in Polymers Electrical Degradation and Breakdown in Polymers*. The Redwood Press, 1992.
- [38] L. A. Dissado, S. J. Dodd, J. V. Champion, P. I. Williams, and J. M. Alison, “Propagation of electrical tree structures in solid polymeric insulation,” *IEEE Trans. Dielectr. Electr. Insul.*, vol. 4, no. 3, pp. 259–279, 1997.
- [39] L. Niemeyer, L. Pietronero, and H. J. Wiesmann, “Fractal dimension of dielectric breakdown,” *Phys. Rev. Lett.*, vol. 52, pp. 1033–1036, 1984.
- [40] H. J. Wiesmann and H. R. Zeller, “A fractal model of dielectric breakdown and prebreakdown in solid dielectrics,” *J. Appl. Phys.*, vol. 60, pp. 1770–1773, 1986.
- [41] S. Kobayashi, S. Maruyama, H. Kawai, H. Uehara, and K. Kudo, “Fractal analysis of 3D reconstructed patterns of real electrical tree,” *Conduct. Break. Solid Dielectr. 1995. ICSD ’95., Proc. 1995 IEEE 5th Int. Conf.*, pp. 299–303, 1995.
- [42] L. A. Dissado, “Understanding electrical trees in solids: From experiment to theory,” *IEEE Trans. Dielectr. Electr. Insul.*, vol. 9, no. 4, pp. 483–497, 2002.
- [43] X. Zheng and G. Chen, “Propagation Mechanism of Electrical Tree in XLPE Cable Insulation by investigating a Double Electrical Tree

- Structure,” *IEEE Trans. Dielectr. Electr. Insul.*, vol. 15, no. 3, pp. 800–807, 2008.
- [44] S. Bahadoorsingh and S. M. Rowland, “The role of power quality in electrical treeing of epoxy resin,” *2007 Annu. Rep. - Conf. Electr. Insul. Dielectr. Phenom.*, pp. 221–224, 2007.
- [45] P. I. Williams and L. A. Dissado, “Physical Origin for differences in Electrical Tree Structures,” in *Annual Report - Conference on Electrical Insulation and Dielectric Phenomena, CEIDP*, 1994, pp. 418–423.
- [46] F. Guastavino, G. Coletti, A. Dardano, A. Ratto, and E. Torello, “Life prediction of XLPE subjected to distorted voltages in presence of bush-like electrical treeing,” in *Electrical Insulation and Dielectric Phenomena, 2006 IEEE Conference on*, 2006, pp. 724–727.
- [47] R. Bozzo, G. Coletti, and F. Guastavino, “Studies About the Electrical Treeing Growth Based on the Evolution of the PD Patterns,” in *IEEE International Symposium on Electrical Insulation*, 1998, pp. 415–419.
- [48] F. Noto and N. Yoshimura, “Voltage and Frequency Dependence of Tree Growth in Polyethylene,” in *Annual Report - Conference on Electrical Insulation and Dielectric Phenomena, CEIDP*, 1974, pp. 207–217.
- [49] M. Ieda, “Dielectric breakdown process,” *IEEE Trans. Electr. Insul.*, vol. EI-15, no. 3, pp. 206–224, 1980.
- [50] N. Shimizu, H. Katsukawa, M. Miyauchi, M. Kosaki, and K. Horii, “THE SPACE CHARGE BEHAVIOR AND LUMINESCENCE PHENOMENA IN POLYMERS AT 77 K,” *IEEE Trans. Electr. Insul.*, vol. EI-14, no. 5, pp. 256–263, 1979.
- [51] K. Nakanishi, S. Hirabayashi, and Y. Inuishi, “Phenomena and mechanisms of Tree Inception in Epoxy Resins,” *IEEE Trans. Electr. Insul.*, vol. EI-14, no. 6, pp. 306–314, 1979.

- [52] J. V Champion, S. J. Dodd, and G. C. Stevens, "Quantitative Measurement of Light Emission During the Early Stages of Electrical Breakdown in Epoxy and Unsaturated Polyester Resins," *J. Appl. Phys.*, vol. 26, pp. 819–828, 1993.
- [53] C. Laurent, "OPTICAL PRE-BREAKDOWN WARNINGS IN INSULATING POLYMERS," in *IEEE International Conference on Conduction and Breakdown in Solid Dielectrics*, 1998, pp. 1–12.
- [54] S. J. Dodd, J. V Champion, and G. C. Stevens, "QUANTITATIVE LIGHT EMISSION AS A PROBE OF ELECTRICAL TREEING PROCESSES," in *IEEE International Conference on Conduction and Breakdown in Solid Dielectrics*, 1992, pp. 308–312.
- [55] C. Laurent, C. Mayoux, and S. Noel, "SPACE CHARGE AND ELECTROLUMINESCENCE IN POLYETHYLENE," *Electr. Insul. 1984 IEEE Int. Conf.*, pp. 13–16, 1984.
- [56] S. S. Bamji, A. T. Bulinski, and R. J. Densley, "THE ROLE OF POLYMER INTERFACE DURING TREE INITIATION IN LDPE," *IEEE Trans. Dielectr. Electr. Insul.*, vol. EI-21, no. 4, pp. 639–644, 1986.
- [57] N. Shimizu and C. Laurent, "Electrical Tree Initiation," *IEEE Trans. Electr. Insul.*, vol. 5, no. 5, pp. 651–659, 1998.
- [58] N. Shimizu, T. Takahashi, and S. Iemura, "INITIATION MECHANISM OF ELECTRICAL TREE UNDER ALTERNATING STRESS - ELECTRON IMPACT OR UV PHOTO-DEGRADATION?," in *International Conference on Solid Dielectrics*, 2001, pp. 423–426.
- [59] T. Tanaka and A. Greenwood, "EFFECTS OF CHARGE INJECTION AND EXTRACTION ON TREE INITIATION IN POLYETHYLENE," *IEEE Trans. Power Appar. Syst.*, vol. PAS-97, no. 5, pp. 1749–1759, 1978.
- [60] F. Guastavino and B. Cerutti, "Tree Growth Monitoring by Means of

- Digital Partial Discharge Measurements,” *IEEE Trans. Dielectr. Electr. Insul.*, vol. 10, no. 1, pp. 65–72, 2003.
- [61] R. Bozzo, C. Gemme, F. Guastavino, M. Cacciari, A. Contin, and G. C. Montanari, “Aging Diagnosis of Insulation Systems by PD Measurements Extraction of Partial Discharge Features in Electrical Treeing,” *IEEE Trans. Dielectr. Electr. Insul.*, vol. 5, no. 1, pp. 118–124, 1998.
- [62] R. Bozzo, A. Contin, C. Gemme, F. Guastavino, and G. C. Montanari, “An Analysis Of The Probability Distributions of Charge In Electrical Trees Generated By Needle Tests,” in *Annual Report - Conference on Electrical Insulation and Dielectric Phenomena, CEIDP*, 1996, pp. 770–774.
- [63] J. V Champion and S. J. Dodd, “An approach to the modelling of partial discharges in electrical trees,” *J. Phys. D. Appl. Phys.*, vol. 31, no. 18, pp. 2305–2314, 1998.
- [64] J. V Champion, S. J. Dodd, and J. M. Alison, “The correlation between the partial discharge behaviour and the spatial and temporal development of electrical trees grown in an epoxy resin,” *J. Phys. D. Appl. Phys.*, vol. 29, no. 10, pp. 2689–2695, 1996.
- [65] R. Bozzo, A. Contin, F. Guastavino, C. Gemme, and G. C. Montanari, “STOCHASTIC ANALYSIS OF PARTIAL DISCHARGE PATTERNS DERIVING FROM ELECTRICAL TREE MEASUREMENTS,” in *International Conference on Conduction and Breakdown in Solid Dielectrics*, 1995, pp. 381–385.
- [66] L. Hui, R. Smith, J. K. Nelson, and L. S. Schadler, “Electrochemical treeing in XLPE/silica nanocomposites,” *Electr. Insul. Dielectr. Phenomena, 2009. CEIDP '09. IEEE Conf.*, pp. 511–514, 2009.
- [67] M. G. Danikas and T. Tanaka, “Nanocomposites - A review of electrical treeing and breakdown,” *IEEE Electr. Insul. Mag.*, vol. 25, no. 4, pp. 19–25, 2009.

- [68] F. Guastavino, A. Dardano, E. Torello, M. Hoyos, J. M. Gomez-Elvira, and P. Tiemblo, “Electrical treeing inception and growth in LDPE nanocomposites,” *Annu. Rep. - Conf. Electr. Insul. Dielectr. Phenomena, CEIDP*, pp. 240–243, 2007.
- [69] M. F. Fréchette, A. Vijh, M. L. Trudeau, D. Fabiani, L. Utracki, S. Gubanski, C. Reed, A. Sami, E. David, J. Kindersberger, A. Krivda, P. Morshuis, T. Andritsch, R. Kochetov, J. Fothergill, S. Dodd, A. S. Vaughan, J. Castellon, and F. Guastavino, “A ‘Universal’ Panacea for Solving All Electrical Insulation Problems ?,” in *International Conference on Solid Dielectrics*, 2010, pp. 1–3.
- [70] T. M. Do, J. L. Augé, and O. Lesaint, “A study of parameters influencing streamer inception in silicone gel,” *IEEE Trans. Dielectr. Electr. Insul.*, vol. 16, no. 3, pp. 893–899, 2009.
- [71] T. M. Do, O. Lesaint, and J. L. Augé, “Streamers and partial discharge mechanisms in silicone gel under impulse and AC voltages,” *IEEE Trans. Dielectr. Electr. Insul.*, vol. 15, no. 6, pp. 1526–1534, 2008.
- [72] O. Lesaint and P. Gournay, “On the gaseous nature of positive filamentary streamers in hydrocarbon liquids. I: Influence of the hydrostatic pressure on the propagation,” *J. Phys. D. Appl. Phys.*, vol. 27, no. 10, 1994.
- [73] P. Gournay and O. Lesaint, “On the gaseous nature of positive filamentary streamers in hydrocarbon liquids. II: Propagation, growth and collapse of gaseous filaments in pentane,” *J. Phys. D. Appl. Phys.*, vol. 27, no. 10, 1994.
- [74] M. Fujii, R. Ueda, H.-G. Jeon, and H. Ihori, “Vibration and Development of Pearl-chain-type Tree in Silicone Gel under AC Voltage *,” in *Conference proceedings of ISEIM*, 2014, pp. 319–322.
- [75] S. J. Dodd, L. M. Salvatierra, L. A. Dissado, and E. Mola, “Electrical Trees in Silicone Gel : A Combination of Liquid and Solid Behaviour Patterns,”

2013 Annu. Rep. Conf. Electr. Insul. Dielectr. Phenom., no. 2, pp. 1018–1021, 2013.

- [76] L. I. Kovalevski and L. M. Salvatierra, “Effect of the field frequency during treeing tests in silicone polymers with different degree of crosslinking,” *2015 Annu. Rep. Conf. Electr. Insul. Dielectr. Phenom.*, pp. 613–616, 2015.
- [77] L. M. Salvatierra, L. I. Kovalevski, P. L. D. Quiña, I. M. Irurzun, and E. E. Mola, “Self-healing during Electrical Treeing : A Feature of the Two-phase Liquid-solid Nature of Silicone Gels,” *IEEE Trans. Dielectr. Electr. Insul.*, vol. 23, no. 2, pp. 757–767, 2016.
- [78] A. C. Ashcraft, R. M. Eichhorn, and R. G. Shaw, “Laboratory Studies of Treeing in Solid Dielectrics and Voltage Stabilization in Polyethylene,” in *IEEE International Conference on Electrical Insulation*, 1976, pp. 213–218.
- [79] E. Details, J. P. Crine, G. C. Stone, M. Kurtz, R. G. van Heeswijk, S. Bahadoorsingh, S. M. Rowland, L. Hui, R. Smith, J. K. Nelson, L. S. Schadler, S. Sambharay, C. Sharma, Xiangrong Chen, A. R. Mantsch, Libin Hu, S. Gubanski, J. Blennow, C.-O. Olsson, N. H. Aziz, V. M. Catterson, M. D. Judd, B. X. Du, T. Han, J. G. Su, L. I. Kovalevski, L. M. Salvatierra, J. V Champion, S. J. Dodd, J. M. Alison, G. Chen, C. H. Tham, W. Ningyan, I. Cotton, J. Robertson, S. Follmann, K. Evans, D. Newcombe, N. Wang, M. G. Danikas, T. Tanaka, L. A. Dissado, P. I. Williams, T. M. Do, O. Lesaint, J. L. Augé, E. Mola, A. S. Preparation, I. Idrissu, G. Mitic, G. Lefianc, G. Salge, and N. Chalashkanov, “Investigating the impact of harmonics on the breakdown of epoxy resin through electrical tree growth,” *IEEE Trans. Dielectr. Electr. Insul.*, vol. 16, no. 4, pp. 511–514, 2009.
- [80] E. Jarvid, A. Johansson, J. Blennow, M. Andersson, and S. Gubanski, “Evaluation of the performance of several object types for electrical

- treeing experiments,” *IEEE Trans. Dielectr. Electr. Insul.*, vol. 20, no. 5, pp. 1712–1719, 2013.
- [81] R. Vogelsang, T. Weiers, and K. Fröhlich, “Electrical Breakdown in High-Voltage Winding Insulations of Different,” vol. 22, no. 3, pp. 5–12, 2006.
- [82] N. Hozumi, M. Ishida, and H. Fukagawa, “The Influence of Morphology on Electrical Tree Initiation in Polyethylene under ac,” *IEEE Trans. Electr. Insul.*, vol. 25, no. 4, pp. 707–714, 1990.
- [83] J. H. Mason, “Breakdown of solid dielectrics in divergent fields,” *Proc. IEE - Part C Monogr.*, vol. 102, no. 2, pp. 254–263, 1955.
- [84] M. Butcher, A. A. Neuber, M. D. Cevallos, J. C. Dickens, and H. Krompholz, “Conduction and Breakdown Mechanisms in Transformer Oil,” *IEEE Trans. Plasma Sci.*, vol. 34, no. 2, pp. 467–475, 2006.
- [85] G. Krause, S. Gottlich, K. Moller, and D. Meurer, “Stress s.,” in *Proceedings of International conference on Conduction and Breakdown in Solid Dielectrics*, 1989, pp. 560–564.
- [86] H. Sakamoto and K. Yahagi, “Electrical Capacitance of Polyethylene under Application of High DC Electric Field,” *Jpn. J. Appl. Phys.*, vol. 19, no. 2, 1980.
- [87] Y. Shibuya, S. Zoledziowski, and J. H. Calderwood, “Light emission and deterioration in epoxy resin subjected to power frequency electric fields,” *Proc. Inst. Electr. Eng.*, vol. 125, no. 4, pp. 352–354, 1978.
- [88] A. C. Ashcraft, “Water treeing in polymeric dielectrics,” in *World Electrotechnical Congress*, 1977.
- [89] A. C. Ashcraft, “Factors influencing treeing identified,” *Electr. world*, 1977.
- [90] T. Baumann, P. Pfluger, F. Stucki, and H. R. Zeller, “CHARGE

INJECTION AND DISTRIBUTION IN POLYMERIC INSULATION SYSTEMS,” in *Annual Report - Conference on Electrical Insulation and Dielectric Phenomena, CEIDP*, 1986, pp. 358–364.

- [91] T. Baumann, B. Fruth, F. Stucki, and H. R. Zeller, “Field-enhancing Defects in Polymeric Insulators Causing Dielectric Aging,” *IEEE Trans. Electr. Insul.*, vol. 24, no. 6, pp. 1071–1076, 1989.
- [92] T. Hibma and H. R. Zeller, “Direct measurement of space-charge injection from a needle electrode into dielectrics,” *J. Appl. Phys.*, vol. 59, no. 5, 1986.
- [93] C. Laurent, C. Mayoux, and S. Noel, “Mechanisms of electroluminescence during aging of polyethylene,” *J. Appl. Phys.*, vol. 52, no. 11, 1985.
- [94] S. S. Bamji, A. T. Bulinski, and R. J. Densley, “Evidence of near-ultraviolet emission during electrical-tree initiation in polyethylene,” *J. Appl. Phys.*, vol. 61, no. 2, 1986.
- [95] R. W. Hare, “Modelling space charge in solid dielectrics,” University of Bristol, 1993.
- [96] J. M. Alison, J. V. Champion, S. J. Dodd, and G. C. Stevens, “Dynamic bipolar charge recombination model for electroluminescence in polymer based insulation during electrical tree initiation,” *J. Phys. D. Appl. Phys.*, vol. 28, pp. 1693–1701, 1995.
- [97] J. Vanderlinede, *Classical Electromagnetic Theory*, 2nd ed. Kluwer Academic Publishers, 2004.
- [98] L. A. Dissado and R. M. Hill, “The Statistics of Electrical Tree Inception,” *IEEE Trans. Electr. Insul.*, vol. 25, no. 4, pp. 660–666, 1990.
- [99] L. Rayleigh, “On the pressure developed in a liquid during the collapse of a spherical cavity,” *London, Edinburgh, Dublin Philos. Mag. J. Sci.*, pp. 94–98, 1917.

- [100] M. S. Plesset, "The dynamics of cavitation bubbles," *J. Appl. Mech.*, vol. 16, pp. 277–282, 1949.
- [101] S. J. Dodd, L. A. Dissado, J. V. Champion, and J. M. Alison, "Evidence for deterministic chaos as the origin of electrical tree breakdown structures in polymeric insulation," *Phys. Rev. B*, vol. 52, no. 24, pp. 985–988, 1995.
- [102] P. Wang, A. Cavallini, G. C. Montanari, and G. Wu, "Effect of Rise Time on PD Pulse Features under Repetitive Square Wave Voltages," *IEEE Trans. Dielectr. Electr. Insul.*, vol. 20, no. 1, pp. 245–254, 2013.
- [103] S. Boggs, "Very High Field Phenomena in Dielectrics," *IEEE Trans. Dielectr. Electr. Insul.*, vol. 12, no. 5, pp. 929–938, 2005.
- [104] M. Sato, A. Kumada, Y. Hayase, K. Yamashiro, Y. Hayase, and T. Takano, "On the nature of surface discharges in silicone-gel: Prebreakdown discharges in cavities," in *Annual Report - Conference on Electrical Insulation and Dielectric Phenomena, CEIDP*, 2014, no. 1, pp. 19–22.